CAMS Service Evolution

D2.1 Report on data assimilation results

Due date of deliverable	31st of December 2024
Submission date	Dec 2024
File Name	CAMEO-D2-1-V2
Work Package /Task	D2.1
Organisation Responsible of Deliverable	ECMWF
Author name(s)	Zoi Paschalidi, Antje Inness, Vincent Huijnen
Revision number	V2
Status	Issued
Dissemination Level	Public

Funded by the European Union

The CAMEO project (grant agreement No 101082125) is funded by the European Union.
Views and opinions expressed are however those of the author(s) only and do not necessarily reflect those of the European Union or the Commission. Neither the European Union nor the granting authority can be held responsible for them.

1 Executive Summary

This report details the integration of satellite retrievals from the GEMS instrument on South Korea's KOMPSAT-2B satellite within the ECMWF Integrated Forecasting System (IFS) framework. The IFS model now accommodates GEMS total O_3 and tropospheric column NO_2 data, which are being routinely monitored in the operational ECMWF CAMS system, starting with model cycle CY49R1. Initial evaluations of the operational GEMS NO_2 version 2 retrievals indicate significant biases, currently restricting their assimilation within the IFS. To address this, an alternative GEMS NO_2 product, based on a new retrieval algorithm developed by the University of Bremen, is under study. This improved GEMS NO_2 product demonstrates enhanced performance and potential for more accurate analysis results. Regarding GEMS O_3 data, observed biases are smaller and align with those from other polar orbiting satellites, indicating potential value in capturing O_3 diurnal variations through data assimilation.

Table of Contents

2 Introduction

2.1 Background

Monitoring the composition of the atmosphere is a key objective of the European Union's flagship Space programme Copernicus, with the Copernicus Atmosphere Monitoring Service (CAMS) providing free and continuous data and information on atmospheric composition.

The CAMS Service Evolution (CAMEO) project will enhance the quality and efficiency of the CAMS service and help CAMS to better respond to policy needs such as air pollution and greenhouse gases monitoring, the fulfilment of sustainable development goals, and sustainable and clean energy.

CAMEO will help prepare CAMS for the uptake of forthcoming satellite data, including Sentinel-4, -5 and 3MI, and advance the aerosol and trace gas data assimilation methods and inversion capacity of the global and regional CAMS production systems.

CAMEO will develop methods to provide uncertainty information about CAMS products, in particular for emissions, policy, solar radiation and deposition products in response to prominent requests from current CAMS users.

CAMEO will contribute to the medium- to long-term evolution of the CAMS production systems and products. The transfer of developments from CAMEO into subsequent improvements of CAMS operational service elements is a main driver for the project and is the main pathway to impact for CAMEO.

The CAMEO consortium, led by ECMWF, the entity entrusted to operate CAMS, includes several CAMS partners thus allowing CAMEO developments to be carried out directly within the CAMS production systems and facilitating the transition of CAMEO results to future upgrades of the CAMS service.

This will maximise the impact and outcomes of CAMEO as it can make full use of the existing CAMS infrastructure for data sharing, data delivery and communication, thus supporting policymakers, business and citizens with enhanced atmospheric environmental information.

2.2 Scope of this deliverable

2.2.1 Objectives of this deliverables

This deliverable reports the progress on the evaluation and integration of geostationary NO_2 and O_3 data from the GEMS satellite, within ECMWF's Integrated Forecast System. GEMS, onboard the South Korean KOMPSAT-2B satellite, is a component of the geostationary Air Quality Constellation, which also includes the American TEMPO instrument and will include the European MTG-S/Sentinel-4 instrument. The report assesses the potential benefits of GEMS data for enhancing the CAMS air quality analyses, detailing the evaluation of GEMS NO_2 and O_3 retrievals in comparison with model outputs and other satellite observations. Initial evaluations of GEMS NO_2 data are presented, including the operational NRT data (version 2) as well as an assessment based on an alternative retrieval approach, developed by the IUP Bremen, aimed at identifying potential improvements. Furthermore, the report provides preliminary results from the first assimilation experiments of GEMS O_3 data, shedding light on the value of geostationary observations for capturing the diurnal cycle of a key air quality component, ozone.

2.2.2 Work performed in this deliverable

In this deliverable the work as planned in the Description of Action (DoA, WPX TY. Z) was performed:

Task 2.1: Assimilation of additional and upcoming satellite retrievals (ECMWF)

2.2.3 Deviations and counter measures

Due to significant biases in tropospheric NO_2, the current operational NRT GEMS NO_2 data was found to be not suitable for assimilation tests. To overcome this issue, an alternative NO_2 product is tested, developed by the University of Bremen, which is expected to have reduced NO_2 biases. This approach allows us to move forward with assimilation work while awaiting improvements in the next version of the operational GEMS NO_2 data.

2.2.4 CAMEO Project Partners:

ECMWF	EUROPEAN CENTRE FOR MEDIUM-RANGE WEATHER FORECASTS
Met Norway	METEOROLOGISK INSTITUTT
BSC	BARCELONA SUPERCOMPUTING CENTER-CENTRO NACIONAL DE SUPERCOMPUTACION
KNMI	KONINKLIJK NEDERLANDS METEOROLOGISCH INSTITUUT-KNMI
SMHI	SVERIGES METEOROLOGISKA OCH HYDROLOGISKA INSTITUT
BIRA-IASB	INSTITUT ROYAL D'AERONOMIE SPATIALEDE BELGIQUE
HYGEOS	HYGEOS SARL
FMI	ILMATIETEEN LAITOS
DLR	DEUTSCHES ZENTRUM FUR LUFT - UND RAUMFAHRT EV
ARMINES	ASSOCIATION POUR LA RECHERCHE ET LE DEVELOPPEMENT DES METHODES ET PROCESSUS INDUSTRIELS
CNRS	CENTRE NATIONAL DE LA RECHERCHE SCIENTIFIQUE CNRS
GRASP-SAS	GENERALIZED RETRIEVAL OF ATMOSPHERE AND SURFACE PROPERTIES EN ABREGE GRASP
CU	UNIVERZITA KARLOVA
CEA	COMMISSARIAT A L ENERGIE ATOMIQUE ET AUX ENERGIES ALTERNATIVES
MF	METEO-FRANCE

TNO	NEDERLANDSE ORGANISATIE VOOR TOEGEPAST NATUURWETENSCHAPPELIJK ONDERZOEK TNO
INERIS	INSTITUT NATIONAL DE L ENVIRONNEMENT INDUSTRIEL ET DES RISQUES - INERIS
IOS-PIB	INSTYTUT OCHRONY SRODOWISKA - PANSTWOWY INSTYTUT BADAWCZY
FZJ	FORSCHUNGSZENTRUM JULICH GMBH
AU	AARHUS UNIVERSITET
ENEA	AGENZIA NAZIONALE PER LE NUOVE TECNOLOGIE, L'ENERGIA E LO SVILUPPO ECONOMICO SOSTENIBILE

3 Incorporating GEMS retrievals in the IFS

The Air Quality Constellation represents a collaborative international effort aimed at advancing the monitoring of air pollution across the Northern Hemisphere with unprecedented spatial and temporal resolution (Committee on Earth Observation Satellites (CEOS), 2019). The constellation consists of three geostationary satellites – GEMS[1], TEMPO[2], and Sentinel-4[3] – deployed by South Korea, the United States, and the European Union, respectively. Together, these satellites will deliver continuous observations of atmospheric pollutants over Asia, North America, and Europe during daylight hours. This coordinated approach will improve our understanding on air quality patterns, pollution sources, and pollutant transport dynamics over north hemisphere, significantly enhancing capabilities for Near-Real-Time (NRT) monitoring and air quality forecasting.

The Geostationary Environment Monitoring Spectrometer (GEMS) (J. Kim et al., 2020; K. Lee et al., 2024), aboard South Korea's KOMPSAT-2B satellite launched in February 2020 marks the first geostationary mission dedicated to observing atmospheric composition over Asia. Unlike traditional polar-orbiting satellites, which provide once-daily measurements, GEMS' geostationary orbit allows for high temporal resolution capturing hourly data over East Asia. This capability includes between 6-7 daylight hours of observations during (local) winter and 7-8 in (local) summer (ranging from 00:45 UTC to 06:45 UTC), with adjustments based on variations in solar zenith angles. GEMS provides high frequency data on key atmospheric pollutants, including NO_2, O_3, SO_2 and aerosols. Its spatial resolution of is approximately 7 x 8 km^2 at the centre of its field of view, effectively capturing regional and urban-scale air quality information across East Asia. Although this spatial resolution is more limited compared to instruments like TROPOMI, GEMS' ability to capture hourly variations provides a fuller picture of daily pollution patterns, being vital for air quality models. Validation campaigns and studies (Baek et al., 2024; Bak et al., 2019; Cho et al., 2024; S. Kim et al., 2023; Lange et al., 2024; Lutz et al., 2023; P. Veefkind et al., 2024) show generally strong correlation between GEMS data and ground-based measurements, confirming its accuracy and reliability for pollutants such as NO_2 and O_3. However, the performance of the current operational GEMS data (version 2) can vary by pollutant and atmospheric conditions (e.g., cloud cover and aerosols). An improved version 3 of GEMS products is planned to be operational by the end of 2025, with preliminary validations indicating promising enhancements in data quality (H. Lee et al., 2024). Consequently, GEMS data provide high-frequency input that enhances the representation of emission sources and daily cycles. This hourly data allows for more accurate forecasting, especially in regions where pollution levels change noticeably over short time frames.

In the CAMS global operational air quality model so far global data from polar orbiting satellites are used. The Tropospheric Modelling Instrument (TROPOMI), aboard the European Sentinel-5P satellite launched in October 2017 (Levelt et al., 2006; J. P. Veefkind et al., 2012), is such a polar-orbiting instrument, designed to measure atmospheric composition globally. TROPOMI, with a spatial resolution of 5.5 x 3.5 km^2, passes once daily over a given location, at 13.30 local solar time, giving one snapshot of traces gases measurements, like NO_2, O_3, SO_2. Numerous studies have demonstrated strong correlations between TROPOMI measurements and ground-based observation in various environments (Douros et al., 2022; Keppens et al., 2024; Lange et al., 2023; van Geffen et al., 2022). Especially for NO_2, as it is of interest for the current report, TROPOMI provides reliable tropospheric column measurements, because it captures spatial gradients and temporal trends effectively, despite the once-daily measurements. As a result, a combined assimilation of polar orbiting and geostationary data, such as GEMS, can crucially advance the atmospheric composition

1 https://nesc.nier.go.kr/en/html/index.do

2 https://tempo.si.edu/index.html

3 https://sentinels.copernicus.eu/web/sentinel/missions/sentinel-4

monitoring and forecasting. The evaluation of such a first implementation is discussed in the followings.

Since April 2023, ECMWF has been acquiring NRT L2 GEMS NO_2 and O_3 data (retrieval version 2). To facilitate integration into the Integrated Forecast System (IFS), report types were assigned to this data, allowing it to be stored in ECMWF's archive for subsequent use (Table 1). The data are converted into BUFR format according to WMO BUFR standards and processed via ECMWF's Scalable Acquisition and Pre-Processing (SAPP) system to handle the data flow efficiently.

Information of GEMS retrievals in ECMWF's Observational Data Base (ODB)			
Satellite	**Sensor**	**Description**	**Report type**
GEO-KOMPSAT-2B satelliteID=814	GEMS instrumentID=689	Retrieved O_3 layers[4]	5097
GEO-KOMPSAT-2B	GEMS	NO_2 Layer integrated mass density with averaging kernels	35023

Table 1: Description of GEMS-KOMPSAT-2B data in the Observational Data Base (ODB) of ECMWF. For more details see https://codes.ecmwf.int/odb/unionall/ .

To ensure compatibility for cycles CY48R1 and CY49R1, several updates were implemented to the system's scripts and source code, facilitating the retrieval, monitoring, and assimilation of GEMS data within the IFS. Specifically, modifications to ECMWF's superobservation software were made to enable efficient handling of the high-volume hourly NRT GEMS observations of NO_2 and O_3 data into the CAMS system, reducing the resolution of the data to the model grid of T511, approximately 40 km x 40 km.

After the initial preparations, a series of data monitoring and evaluation experiments were conducted with the IFS, as detailed in subsequent sections. The primary objective of the monitoring experiments is to validate the technical implementation and to rigorously assess the quality of GEMS data. This evaluation includes comparison with other satellite data, model outputs, and independent observations to confirm accuracy and reliability. Once the data quality is confirmed, assimilation experiments are conducted to assess the impact of these new observations on the accuracy and performance of analysis and forecast outputs.

Upon successful validation of the technical implementation, GEMS L2 v.2 data was included in the CY49R1 model cycle, that became operational on 12 November 2024 and GEMS monitoring plots are now available from the CAMS website:

https://atmosphere.copernicus.eu/charts/packages/cams_monitoring/?facets=%7B%22Instrument%22%3A%5B%22GEMS%22%5D%7D

4 Currently there are no available averaging kernels for GEMS Ozone column retrievals

4 Evaluation of GEMS NO_2 observations

GEMS provides hourly observations of NO_2 columns with high spatial resolution over East Asia, which are processed through the operational GEMS NO_2 retrieval algorithm version 2.0 (Lee Hanlim et al., 2020). The operational retrieval combines advanced radiative transfer modelling with state-of-the-art spectral fitting techniques in three main steps: First the retrieval of the NO_2 Slant Column Density (SCD) based on the Differential Optical Absorption Spectroscopy (DOAS) technique takes place, followed by the calculation of the Air Mass Factor, in order to convert the SCD to Vertical Column Densities (VCD). Here the radiative transfer model of the retrieval considers different parameters, such as the aerosol optical depth, the terrain reflectivity, the albedo or the solar zenith angles, to end up with individual AMFs for total, stratospheric and tropospheric NO_2. Finaly, the tropospheric and stratospheric NO_2 columns are separated, by subtracting the estimated stratospheric column from the total NO_2 column, while using a-priori information from the WRF-Chem chemical transport model, as well as statistical interpolation methods.

The GEMS NO_2 retrievals capture NO_2 hotspots, like urban and industrial areas in Korea, Japan and China, while having strong consistency with existing satellite products (like OMI) and high correlation with ground-based measurements – like MAX-DOAS and Pandora networks (Li et al., 2023; Seo, Kim, et al., 2024). However, hotspot regions can influence the stratospheric-tropospheric separation and end up with elevated tropospheric NO_2 values (Boersma et al., 2004; Lorente et al., 2017; Zhang et al., 2023). The retrieval also shows sensitivity to aerosols, cloud cover and meteorological data that can introduce important uncertainties in the final product, especially over heterogenous surfaces, like urban and industrial areas, or mountainous regions and coastlines (B.-R. Kim et al., 2024; Seo, Valks, et al., 2024).

The upcoming version 3 of the GEMS retrieval algorithm is expected to become operational around the end of 2025 and aims to address many of these issues. Validation processes (including campaigns using diverse ground-based and airborne datasets) verify improvements in cloud and aerosol correction schemes, in surface reflectance treatment and the consistency of the diurnal cycles (H. Lee et al., 2024).

During the period covered by this deliverable, the primary focus was on evaluating the current operational GEMS v2.0 NO_2 product within the CAMS system and assessing its potential to enhance NO_2 analysis and forecasting. This evaluation began with comprehensive monitoring of the GEMS NO_2 data within the IFS. After converting the data into BUFR format, it was introduced into the CAMS data assimilation system. That was feasible as the averaging kernels of the GEMS NO_2 retrievals were available and the IFS advanced observation operators could be applied. These observation operators utilise averaging kernels to integrate model simulations with satellite retrievals (Inness et al., 2022). The retrieval process is represented mathematically as:

$$y_o = x_{ap} + A\left(x_t - x_{ap}\right) + \epsilon\,,$$

where y_o is the retrieved column, here of GEMS NO_2, x_t is the true vertical profile, x_{ap} is the a-priori profile used in the retrieval, A is the averaging kernel and ϵ represents measurement and forward model errors. For each observation the model is interpolated to the specific time and location of the observation and the model's first guess x_m is calculated by applying the averaging kernels to smooth the vertical profile according to the observation's sensitivity. In the observation operator, the averaging kernels are applied to the model profiles to smooth them according to the sensitivity of the retrieval, removing the influence of the a priori profile in the calculation of the departures:

$$d = A\left(x_t - H(x_m)\right) + \epsilon\,.$$

This first guess serves as the basis for initializing the short-range forecast. By incorporating the averaging kernels, the observation operator ensures consistency between the modelled and retrieved profiles, improving the representation of NO_2 concentrations. If averaging kernels are unavailable for a specific observation, the first guess is calculated using a simpler method; as a vertical integral of the model's profile between the bounding pressure levels of the retrieval. This way ensures that the assimilation system remains robust in the absence of averaging kernels, with reduced though sensitivity to the specific characteristics of the retrieval.

The first-guess departures (differences between the first guess and the observations) are crucial for assessing data quality. These departures provide a refined perspective on day-to-day variations in model errors and biases, as they are typically smaller than the observed values. This diagnostic information is essential in identifying strengths and weaknesses of both the data and the model, paving the way for targeted improvements in NO_2 analysis and forecast performance within the CAMS framework (Inness et al., 2019).

4.1 Near Real Time GEMS NO_2 tropospheric column data

The evaluation period spans 12 months, from September 1, 2023, to September 1, 2024, focusing on the IFS-COMPO assimilation experiment 0079 (Table 2) of the cycle CY49R1 experimental suite. This experiment incorporates the configuration of the operational CAMS NRT analysis, which was activated on 12 November 2024. Throughout this period, NRT GEMS NO_2 and O_3 observations are systematically monitored to assess their integration and performance within the CAMS framework.

Experiments evaluated			
Experiment ID	**Evaluated period**	**Evaluated GEMS data**	**GEMS data use**
0079	20230601 – 20240901	NRT NO_2 & O_3	monitor
ihem	20230901 – 20241001	NRT NO_2	monitor
iiy1	20230901 – 20241001	IUP-UB NO_2 retrievals	monitor
igae	20240101 – 20240625	NRT O_3	assimilation

Table 2: Description of the IFS experiments that are evaluated for the scopes of the current deliverable. NRT GEMS data refer to the operational GEMS data from NIER, IUP-UB data refer to the scientific GEMS data produced by the University of Bremen.

Data regions evaluated				
Area name	**LatS**	**LatN**	**LonW**	**LonE**
GEMS area	-10.0	50.0	70.0	150.0
Beijing area	30.0	50.0	110.0	130.0
Korea area	30.0	50.0	120.0	140.0
Tibetan Plateau	30.0	50.0	70.0	110.0
Taiwan area	15.0	30.0	105.0	130.0
India area	0.0	40.0	60.0	100.0

Table 3: Description of the regions presented in the evaluation plots.

The evaluation of GEMS NO_2 data through comparisons with the model first guess and TROPOMI observations underscores key temporal and spatial differences between the two satellites. The continuous temporal coverage of GEMS, allows for hourly data collection over East Asia, capturing dynamic changes in NO_2 concentrations throughout the day along the whole domain. In contrast, TROPOMI, as a polar-orbiting satellite, provides discrete passes over the same area, with its observations limited to specific times and regions.

Figure 1 shows an example of observation snapshots for 01.09.2023 for both TROPOMI (left column) and GEMS (right column) during daylight hours over the GEMS domain. It is highlighted that while GEMS collects continuous hourly data across the entire domain, TROPOMI observations are restricted to its orbital path, resulting in fragmented spatial coverage and time-specific data acquisition.

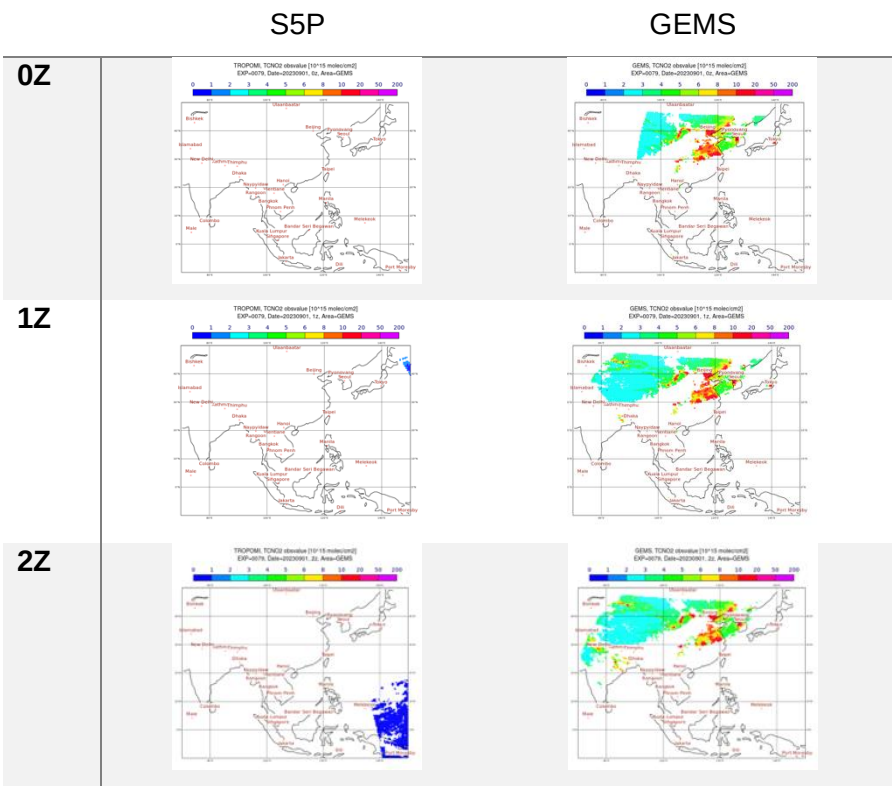

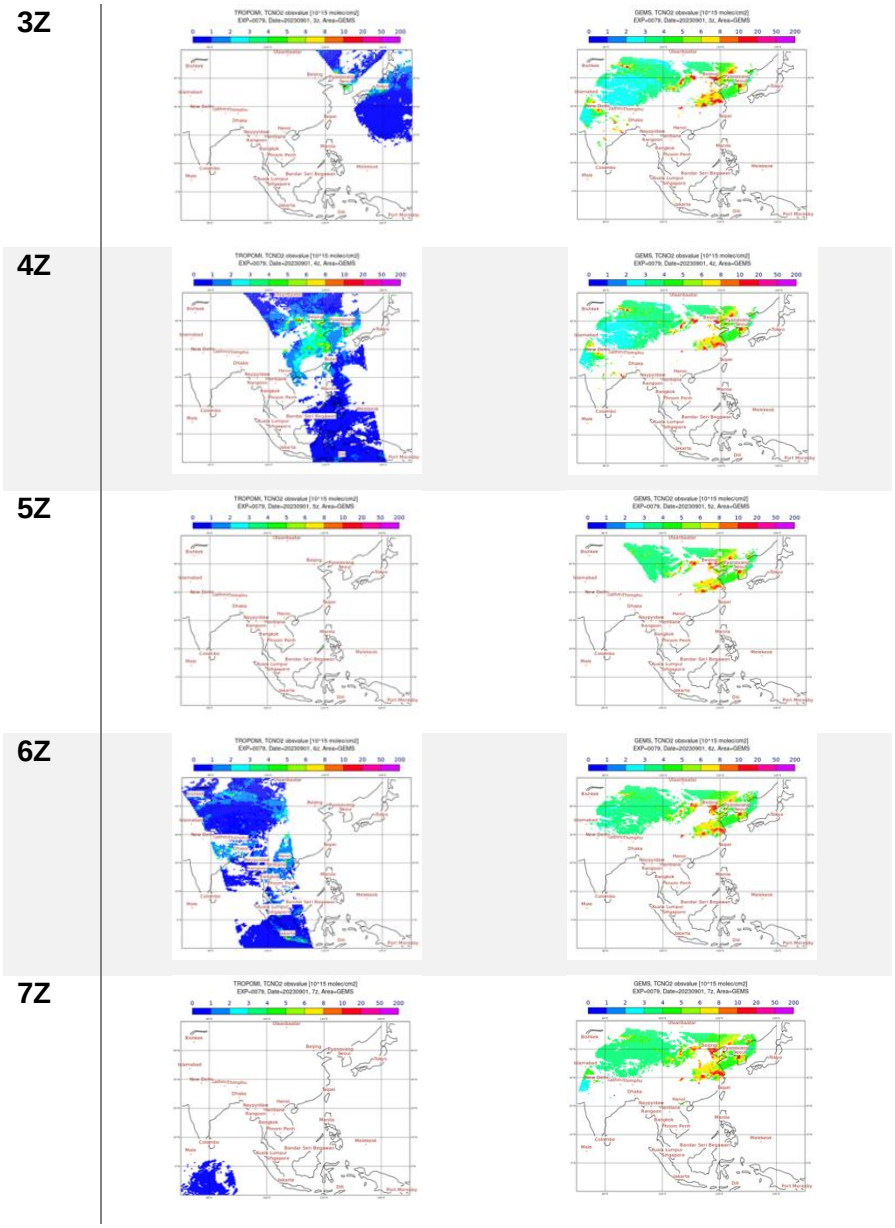

Figure 1: Observation snapshots of TROPOMI (left column) and GEMS (right column) NO_2 measurements in 10^{15} molec/cm^2 over GEMS domain for 1st September 2023 and different times during daylight (2z refers to 02:00 in UTC etc).

Having clarified the basic steps of the methodology followed in the current study, the evaluation of NO_2 GEMS data monitoring through the CAMS experimental suite is presented next.

Figure 2 shows the timeseries of daily mean tropospheric column NO_2 data from GEMS and TROPOMI over the GEMS domain for the entire analysis period (see Table 1 for details). The timeseries indicate that GEMS observations exhibit a consistent high bias throughout the year when compared to TROPOMI data. GEMS data have higher NO_2 levels overall, reaching maximum values of 0.9×10^{-5} molec/cm^2, while TROPOMI levels remain below 0.2×10^{-5} molec/cm^2. Additionally, GEMS data show significant variability while the TROPOMI data demonstrate much lower overall variability. Moreover, GEMS observations show a clear seasonal pattern, more pronounced than for TROPOMI, with peaks around December to

January, followed by a gradual decrease until around April, after which the values stabilise at a lower level.

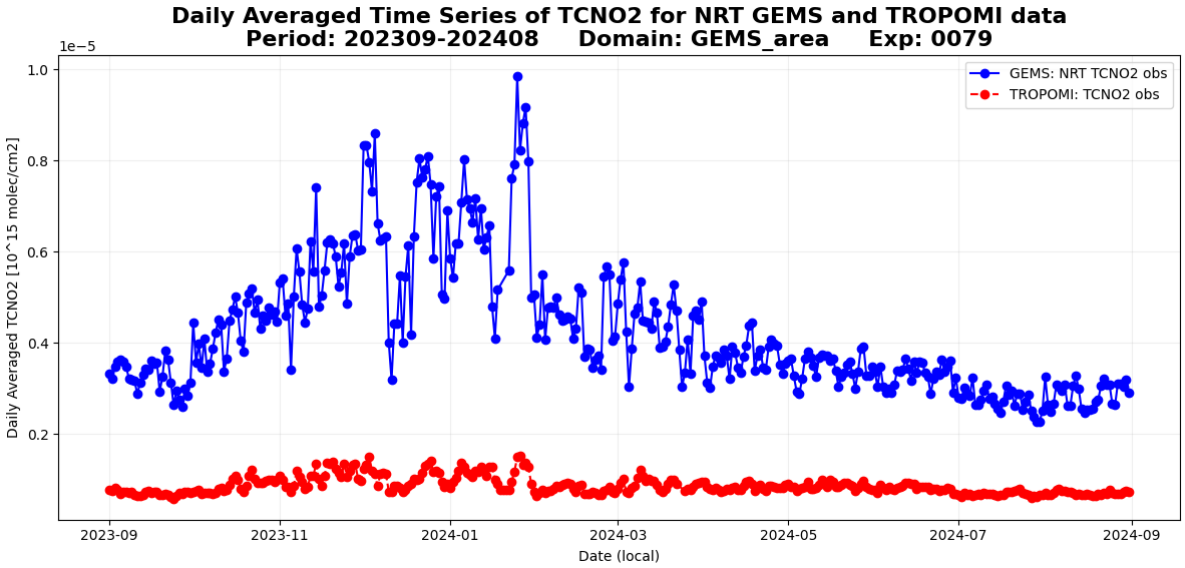

Figure 2: Yearly timeseries of NO_2 tropospheric column observations (given in 10^{15} molec/cm^2) as daily averaged values for GEMS (in blue) and TROPOMI (in red) satellites, from 1st of September 2023 to 1st September 2024 over the GEMS domain. Date information given in local time.

Figure 3 presents maps of the first guess departures for GEMS (left panel) and TROPOMI (right panel) observations over the GEMS domain, averaged over the study period. In case of TROPOMI, the first guess departures display relatively small deviations, with a mean close to zero (0.050 x 10^{15} molec/cm^2), indicating good agreement between the TROPOMI observations and the model background. Slight positive biases (red) are observed in urbanized or industrial regions, especially over northeastern China, which may indicate areas with high anthropogenic emissions. Negative biases (blue) are found in parts of Southeast Asia and some oceanic regions, suggesting lower observed NO_2 levels than the model's forecast. In case of GEMS data, departures are larger, with a mean of –1.83x10^{15} molec/cm^2. Significant positive biases (red) are concentrated in high-emission regions, including northeastern China and parts of Southeast Asia.

According to so far published evaluation studies and personal communications with the Korean data provider (Baek et al., 2023; Bak et al., 2013; B.-R. Kim et al., 2024; Park et al., 2023) these biases result from issues in the retrieval process of the current data retrieval version 2.0. Specifically, the technique used to separate stratospheric and tropospheric NO_2 tends to overestimate tropospheric NO_2 columns while underestimating stratospheric values. Additionally, the retrieval method assumes higher emissions in urban areas, which contributes to elevated NO_2 levels in those regions. Conversely, large negative biases appear along coastlines and at northern latitudes, attributed to limited geographic information in the retrieval process. These issues in GEMS NO_2 data version 2.0 have been validated by the data provider (S. Kim et al., 2023) and corroborated by other studies (Lange et al., 2024; Lutz et al., 2023; Richter et al., 2024; Seo, Valks, et al., 2024).

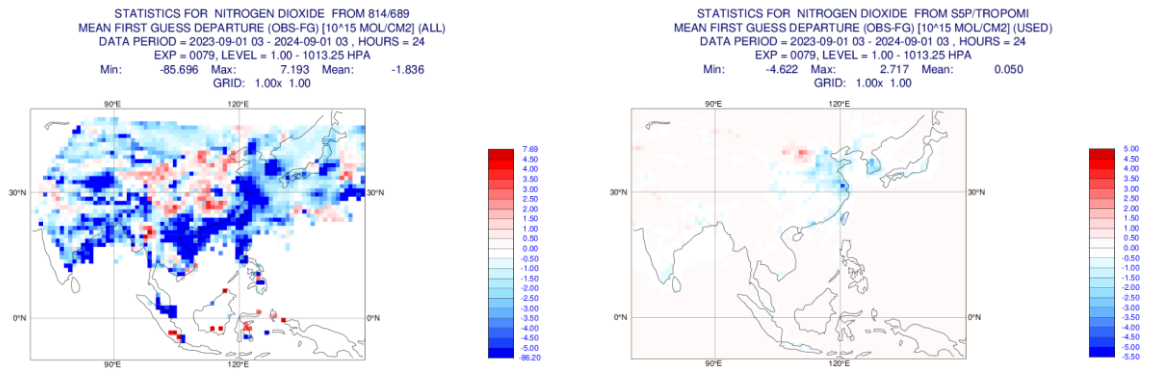

Figure 3: Map plots over the area that GEMS satellite covers, referred in the report as GEMS domain. Mean first guess departures (observation-minus-model's first guess) of GEMS (left panel) and TROPOMI (right panel) satellites, as daily means over a year of calculation (01.09.2023 - 01.09.2024). The colour bar gives the NO_2 differences as 10^{15} molec/cm^2).

A closer examination of the data distribution is provided in Figure 4a, which displays histograms of the GEMS and TROPOMI first guess departures, covering a 12-month period over the Northern Hemisphere. TROPOMI (pink) shows a distribution centred around zero, with a mean departure of 0.1 molec/cm^2 and a small root mean square (RMS) error equal to 0.5 molec/cm^2, indicating good agreement with the model background. In contrast, GEMS (blue) exhibit a broader distribution, with mean value of –1.8 molec/cm^2 and a notably higher RMS error of 8.3 molec/cm^2, suggesting greater deviations from the model.

The differences in spread and central values between the two datasets reveal biases, further highlighted in the box plots in Figure 4b for the first guess departures and 4c for the observation themselves. In Figure 4c the GEMS observations (blue) show a wider spread and several outliers, indicating greater variability. TROPOMI (pink), on the other hand, has a more compact distribution with a narrower range, reflecting more consistent measurements.

a)

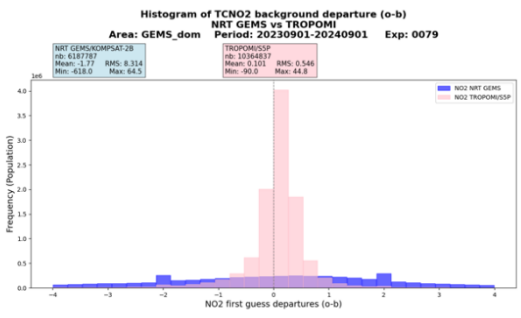

b)

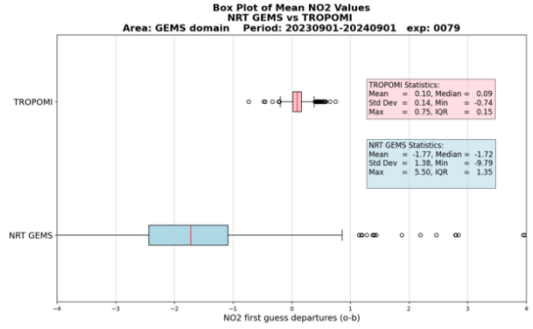

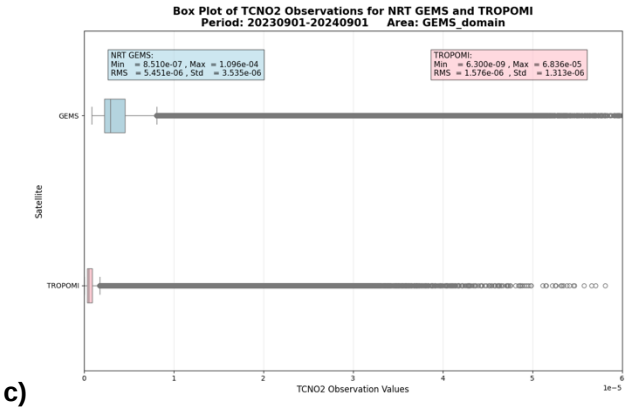

c)

Figure 4: Evaluation of the data bias: Histogram (a) of the first guess departures for GEMS (blue) and TROPOMI (pink) over a year of calculations (from 1st of September 2023 to 1st of September 2024.) of the CAMS experiment; Box plot of the mean first guess departures (4b) and of the observations (4c) (in molec/cm^2) of the same period for GEMS (blue) and TROPOMI (pink).

The analysis of GEMS data can identify the seasonal variations as well as pollution events with higher temporal resolution than TROPOMI – that only passes daily over the GEMS area. This fact is illustrated in Figure 5, which displays seasonal timeseries of NO_2 measurements for each quarter (i.e. DJF, MAM, JJA, SON). Across all seasons, the timeseries highlight significant discrepancies in the observed NO_2 levels between the two satellites. GEMS data demonstrate substantial variations over short periods, with peak values appearing in late October 2023 and mid-January 2024 (5a and 5b), when anthropogenic emissions, atmospheric stability and increased chemical lifetime contribute to elevated NO_2 levels. TROPOMI, in contrast, maintains a steadier and lower baseline for NO_2 levels across both periods. In MAM and JJA (5c and 5d) GEMS observations show a lower bias than in DJF compared with TROPOMI but still show considerable variability.

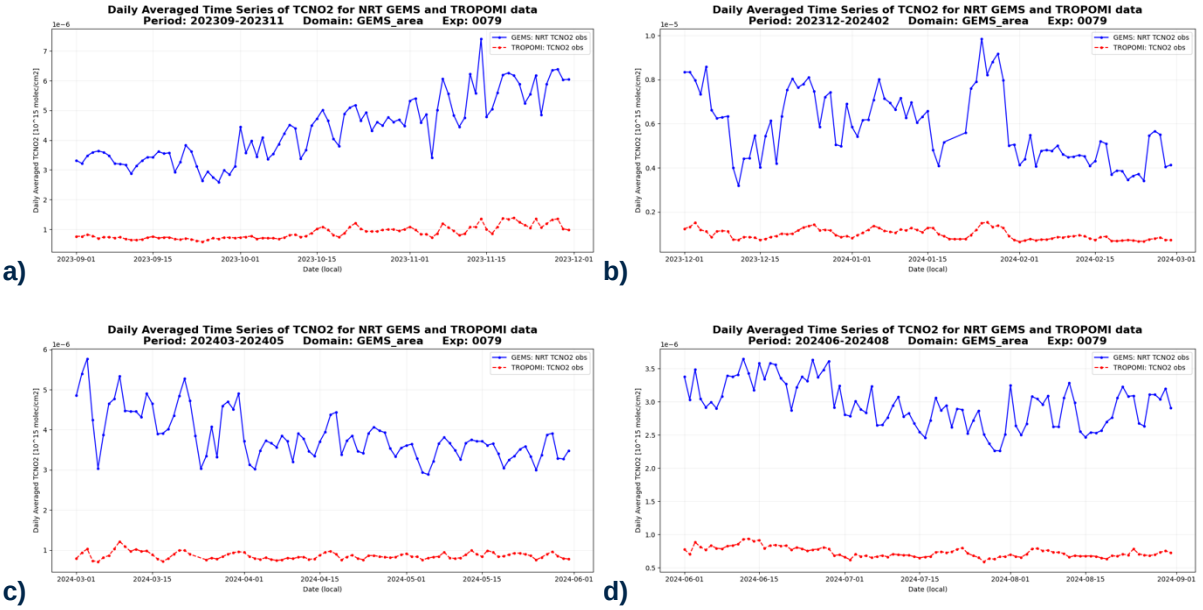

a) b) c) d)

Figure 5: Daily averaged timeseries over GEMS area of satellite observations for every season in the evaluated period (1st of September 2023 to 1st of September 2024) (Lines as; (a): SON, (b): DJF, (c): MAM (d): JJA). The blue lines refer to GEMS data and the red to TROPOMI data.

To investigate the local-scale biases in GEMS data, a smaller domain centred around Beijing is analysed. Figure 6 presents the seasonal distribution of NO_2 observations from GEMS and TROPOMI over an extended Beijing area (see Table 3 for domain specifications). Throughout the year, a prominent positive bias is observed in the GEMS NO_2 measurements over this urban region, with a notable increase during late 2023 and beginning 2024. During DJF, GEMS consistently reports higher NO_2 concentrations compared to TROPOMI, amplifying the bias.

This persistent high bias in GEMS data over a densely populated and high-emission area is mainly linked to specific characteristics that have been identified in the version 2 GEMS retrieval, as already discussed (Edwards et al., 2024). Assumptions like the high aerosol concentrations over cities or the tropospheric-stratospheric separation scheme contribute to an overestimation of NO_2 levels in areas with significant anthropogenic emissions, such as Beijing.

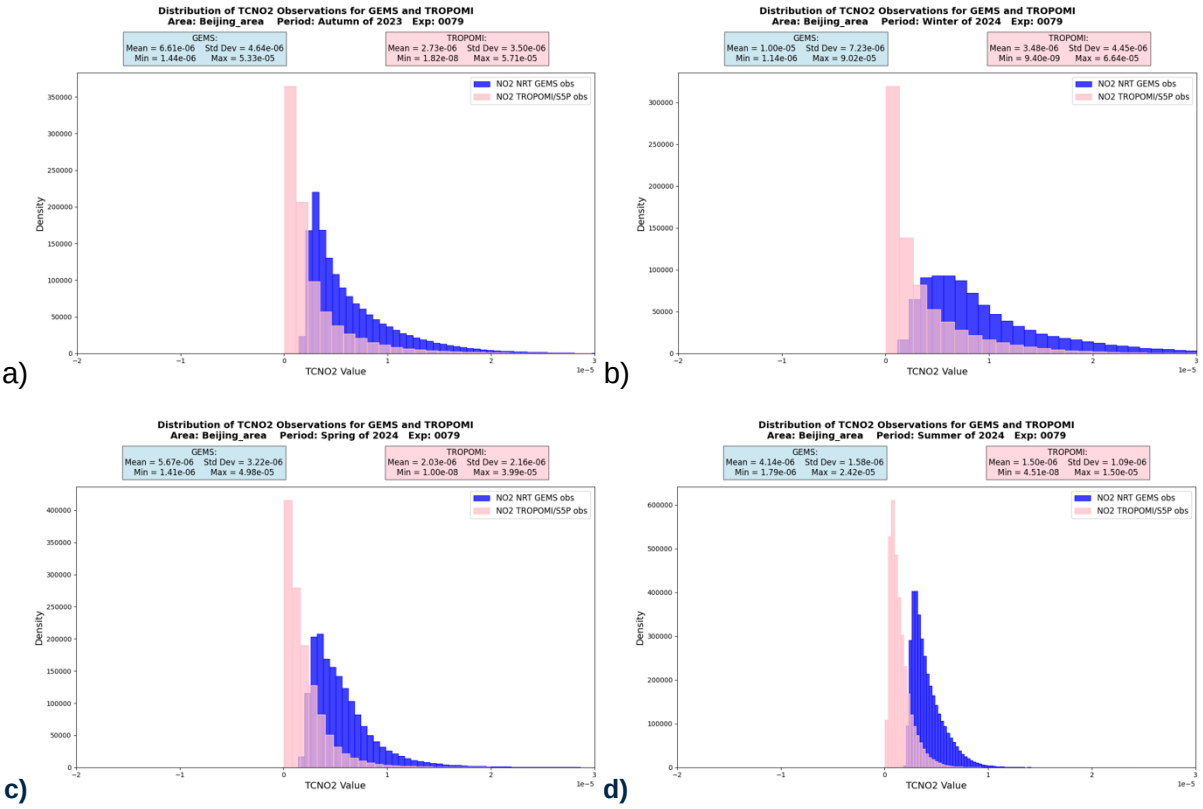

Figure 6: Histograms of NO_2 GEMS (blue) and TROPOMI (red) observations over extended Beijing area by season: (a) SON 2023, (b) DJF 2024, (c) MAM 2024 and (d) JJA 2024

This effect can be also verified by maps of the first guess departures for the area. GEMS (Figure 7a) shows positive biases, especially over Beijing and the urban area of the Tianjin port in China. The strong negative biases along coastal regions and certain inland areas indicate potential underestimations in observed NO_2 levels compared to the forecast but also to the TROPOMI NO_2 observations, as is indicated by the first guess departures on Figure 7b possibly be explained by to retrieval limitations in capturing geographic variability, or the influence of the cloud cover information and the stratospheric-tropospheric separation (B.-R. Kim et al., 2024).

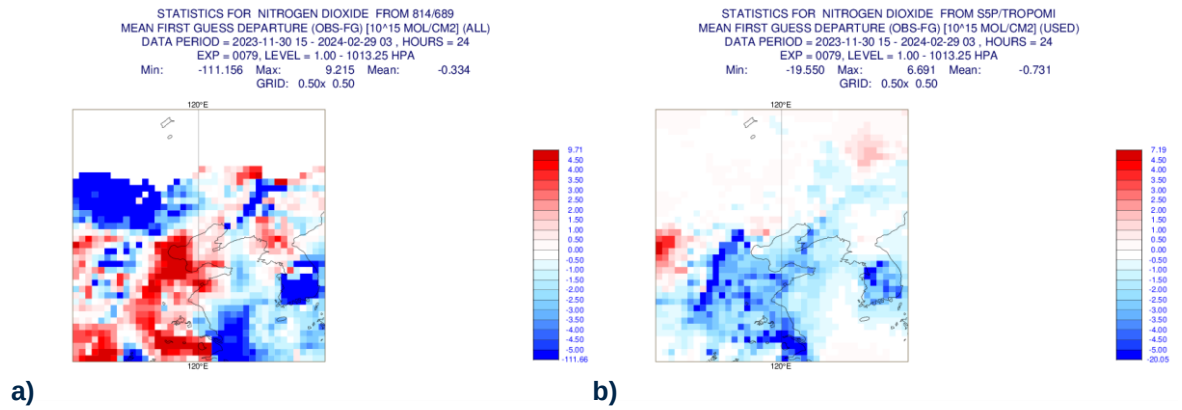

Figure 7: Map plots over the extended Beijing area for DJF 2024. Mean first guess departures (observation-minus-model's first guess) of GEMS (a) and TROPOMI (b) satellites, as daily means over the period 01.12.2023-29.02.2024.

The diurnal cycle plots for each season over the Beijing area (Figure 8) reveal significant patterns in NO_2 concentration dynamics as observed by GEMS and predicted by the IFS model. The GEMS NO_2 observations (in blue) demonstrate a clear diurnal variation with a peak occurring typically in the late morning (around 09:00-11:00 local time). This aligns with the morning rush hour emissions and the atmospheric boundary layer dynamics, where pollutants are trapped closer to the surface. However, the IFS first guess systematically overestimates the measured NO_2, which points to the issues with the version 2.0 data retrieval: whereas GEMS data is already expected to be biased high, the first guess values are even higher, likely due to erroneous averaging kernel values. Despite the bias of GEMS data, the figures underline the added value of GEMS hourly data for improving the model diurnal cycle and its emission estimation.

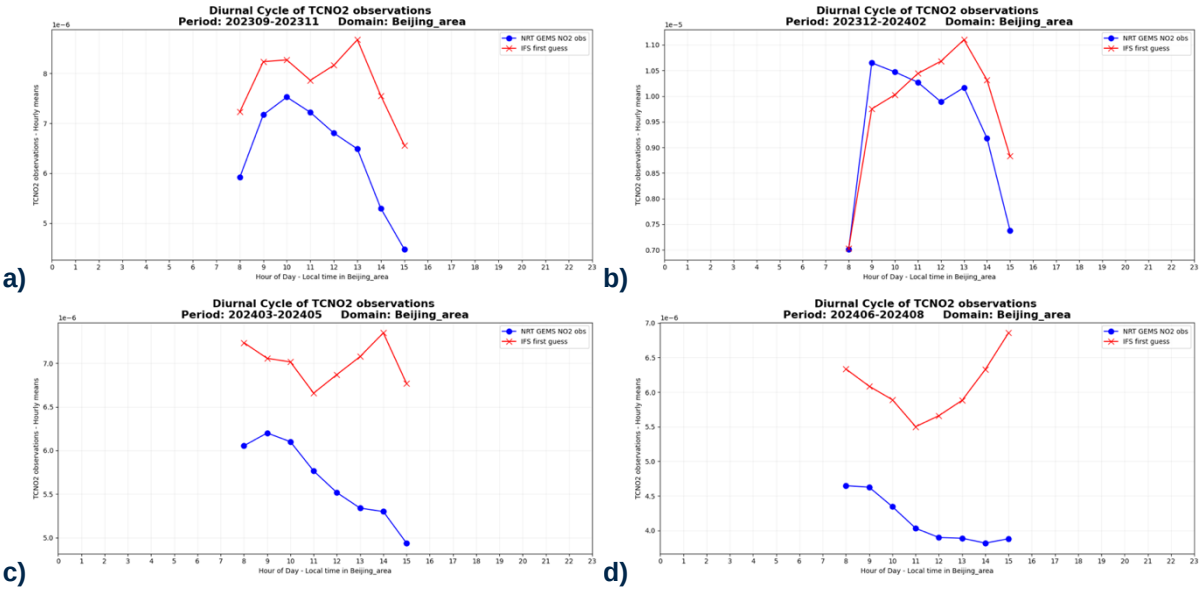

Figure 8: Diurnal cycle of NO_2 GEMS observations (blue) and the IFS first guess (red) over extended Beijing area, in local time, by season: (a) SON 2023, (b) DJF 2024, (c) MAM 2024 and (d) JJA 2024

The significant NO_2 biases identified thus far have prevented the successful assimilation of GEMS tropospheric NO_2 retrievals within the CAMS system. The current GEMS NO_2 data would fail to pass the quality control checks. As a result, no assimilation evaluation has been

performed. It is anticipated that the upcoming version 3 of the GEMS retrieval algorithm will address these issues, allowing for future assessments and potential integration of the data into the CAMS assimilation system.

4.2 GEMS NO_2 tropospheric column retrieval from IUP Bremen

The described large biases in tropospheric NO_2 seen in the operational NRT GEMS data have so far made assimilation tests with the data impossible. To overcome these limitations, an alternative NO_2 product from the Institute of Environmental Physics of the University of Bremen (Lange et al., 2024; Richter et al., 2024) was acquired and is now being tested, in the hope of being able to carry out meaningful assimilation tests with the data.

The Institute of Environmental Physics at the University of Bremen (IUP-UB) has developed a new tropospheric NO_2 product based on the GEMS L1 spectra, known as the scientific GEMS IUP-UB tropospheric NO_2 product v.1.0. This product includes a broader spectral range, and specific adjustments tailored for upcoming European missions, whereas the operational product prioritizes real-time applications with higher-resolution modelling for NO_2 data.

Lange et al. (2024) shows that IUP-UB tropospheric NO_2 product has improved data quality compared to the operational NRT L2 GEMS retrieval algorithm and aligns with TROPOMI measurements. Key enhancements include a larger spectral fitting window, polarization correction, adjustments for scene inhomogeneity, and improved cloud fraction calculations. Table 4 highlights the main differences between the two products. Among them, the stratospheric correction and the surface reflectivity treatment are the primary drivers of the discrepancies. The NRT L2 GEMS product often uses a stratospheric correction that is too low, leading to an overestimation of tropospheric NO2 columns, while the IUP-UB product applies a more refined stratospheric correction, which improves accuracy and reduces the bias. Moreover, the operational GEMS product uses a less accurate reflectivity parametrization, contributing to the scatter and overestimation observed, when the IUP-UB product employs more accurate reflectivity assumptions having significant impact on the NO2 retrievals.

	Operational NRT GEMS L2 NO_2 VCD product v2.0	Scientific GEMS IUP-UB tropospheric NO_2 VCD product v1.0
Fitting window	432-450 nm (DOAS fit)	405-485 nm with additional corrections for polarization sensitivity and scene inhomogeneity
Modelling and profile Shapes	GEOS-Chem model with a high spatial resolution (0.25° × 0.3125°) for the conversion from NO_2 SCDs to VCDs	TM5 model with a lower spatial resolution (1° × 1°) for profile shapes
Air Mass Factor (AMF) Calculations	AMFs from the VLIDORT model, considering factors like solar zenith angle (SZA), surface albedo from GEMS data, and various atmospheric parameters	AMFs computed with the SCIATRAN model, also accounting for SZA and other factors. The default albedo source is TROPOMI's Lambertian equivalent reflectivity climatology
Cloud Correction	Cloud correction by weighting clear-sky and cloudy AMFs based on cloud radiance fraction	independent pixel approximation for cloud correction, recalculating cloud fractions and pressures based on the GEMS cloud product
Aerosol Treatment	Includes aerosol parameters from GEMS L2 data, such as aerosol optical thickness and single scattering albedo	No aerosol correction

Stratospheric – tropospheric separation	Based on Bucsela et al. (2013)	Based on Stratospheric Estimation Algorithm from Mainz (STREAM; Beirle et al., 2016)
Quality Control	Observations with cloud fraction >0.3 are excluded and a final algorithm flag of 1 is used	Observations with cloud radiance fraction >0.5 are discarded - quality assurance value above 0.75 is required
Error Estimation	Both products estimate a tropospheric NO_2 VCD error of ±25%, but this only accounts for uncertainties in AMF calculations	

Table 4: The main differences between the operational NRT GEMS tropospheric NO_2 retrieval and the scientific one developed by IUP-UB.

A one-year test dataset for 2023 has been provided by the University of Bremen for use in the CAMEO project. This dataset underwent the same processing as the NRT GEMS data at ECMWF, including conversion to BUFR format and storage in the data bank for further analysis. However, unlike the NRT data, the Bremen dataset does not include averaging kernels for the NO_2 retrievals. Therefore, the model's first-guess is calculated as simple vertical integral up to the tropopause, defined as the level folding between the bottom (100hPa) and top pressure (1013hPa) levels based on the temperature lapse rates.

Following this preparatory work, IFS experiments were set up to evaluate the scientific IUP-UB NO_2 dataset.

4.2.1 GEMS IUP-UB NO_2 monitoring

For a better understanding of the different datasets, Figure 9 presents NO_2 measurements from three sources; the IUP-UB GEMS product (a), the NRT GEMS (b) and the TROPOMI (c) products. Despite being derived from the same GEMS spectra, plots (a) and (b) exhibit notable differences due to the distinct retrieval algorithms used to process the initial spectra data. The IUP-UB GEMS product provides high spatial resolution and dense coverage across the GEMS domain, enabling the clear identification of major and minor pollution sources and high populated urban areas. Conversely, the NRT GEMS NO_2 dataset also offers high spatial resolution, pointing prominent NO_2 emission regions (Fig. 9b), but shows reduced observation density, with large areas of the domain without any information - as it is seen in the monthly mean of the observation number (Figure 9e). The TROPOMI data on the other hand, provide smooth and consistent information about the NO_2 levels over large areas of the domain (Figure 9c and 9f), being in good agreement with IUP-UB data set (Figure 9a and 9d).

As already discussed in Section 4.1, the operational NRT GEMS data have higher NO_2 values than TROPOMI, particularly over densely populated and industrialized regions in northeast China. In contrast, the IUP-UB GEMS data agree better with the TROPOMI observations

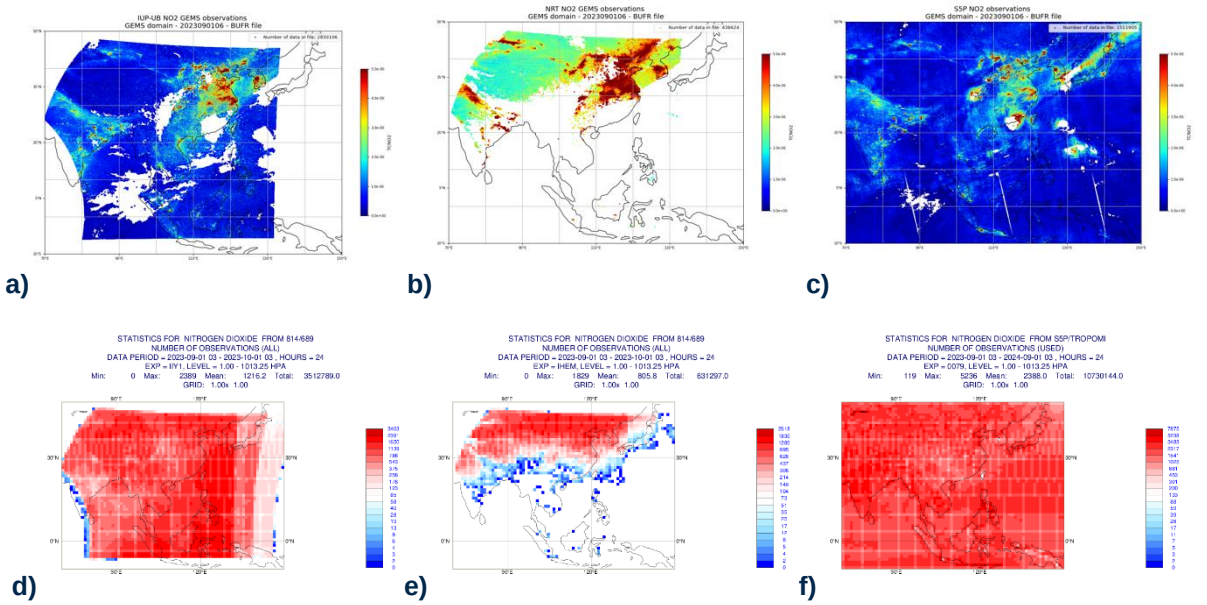

Figure 9: GEMS NO_2 concentrations over east Asia (GEMS-satellite-view domain) as captured in the BUFR files of the IUP-UB NO_2 GEMS data set (a), NRT NO_2 GEMS (b), and NO_2 TROPOMI (c) for 01.09.2023 at 06:00 UTC and mean number of observations over a month of the evaluation period; (d): IUP-UB NO_2 GEMS, (e): NRT NO_2 GEMS and (f): NO_2 TROPOMI.

The performance of the two GEMS data products is examined against the equivalent TROPOMI dataset, using the IFS experiments **ihem** and **iiy1** of cycle CY49R1 (Table 2). Both experiments use the operational CAMS configuration and monitor the GEMS dataset passively, with experiment **ihem** using the NRT NO_2 GEMS data and experiment **iiy1** the IUP-UB NO_2 ones.

A comprehensive, year-long evaluation of these data products for 2023 is currently in progress. However, for the scopes of the present report, a preliminary assessment has been conducted for a one-month test period in September 2023. This shorter-term analysis provides initial insights into the comparative accuracy and reliability of the operational and scientific GEMS NO_2 data products in relation to the TROPOMI dataset.

Figure 10 presents an observation statistics analysis of the aforementioned experiments, providing information into the daily mean NO_2 observation values (left panels) and the daily mean discrepancies with the first guess departures (right panels). The IUP-UB GEMS dataset shows a mean NO_2 concentration of 1.27×10^{15} molec/cm^2, relatively close to the TROPOMI value of 0.87×10^{15} molec/cm^2. In contrast, the mean for the NRT GEMS is 4.3×10^{15} molec/cm^2, indicating a positive bias for the latter. The IUP-UB GEMS spatial distribution of high NO_2 levels is more confined, focusing on specific regions of high pollution, in a similar pattern as the TROPOMI.

The daily mean differences between observed NO_2 concentrations and the first guess model values (observations minus forecast) show smaller departures for TROPOMI and IUP-UB GEMS data than the NRT GEMS data. In case of NRT GEMS NO_2 significant departures are highlighted; positive around polluted regions (e.g. Beijing) and strong negative along coastlines. In case of IUP-UB GEMS NO_2 the first guess departures, while showing improvement compared to the NRT GEMS product, remain larger than those of the TROPOMI dataset, possibly mainly due to the different spatial and temporal coverage characteristics of the two satellites. GEMS observations provide higher temporal resolution with multiple measurements per day, that despite being a great advantage can introduce additional variability due to cloud cover, diurnal changes or retrieval sensitivities, whereas TROPOMI,

with a single overpass per day, captures a more consistent snapshot, potentially reducing the variability in the departures.

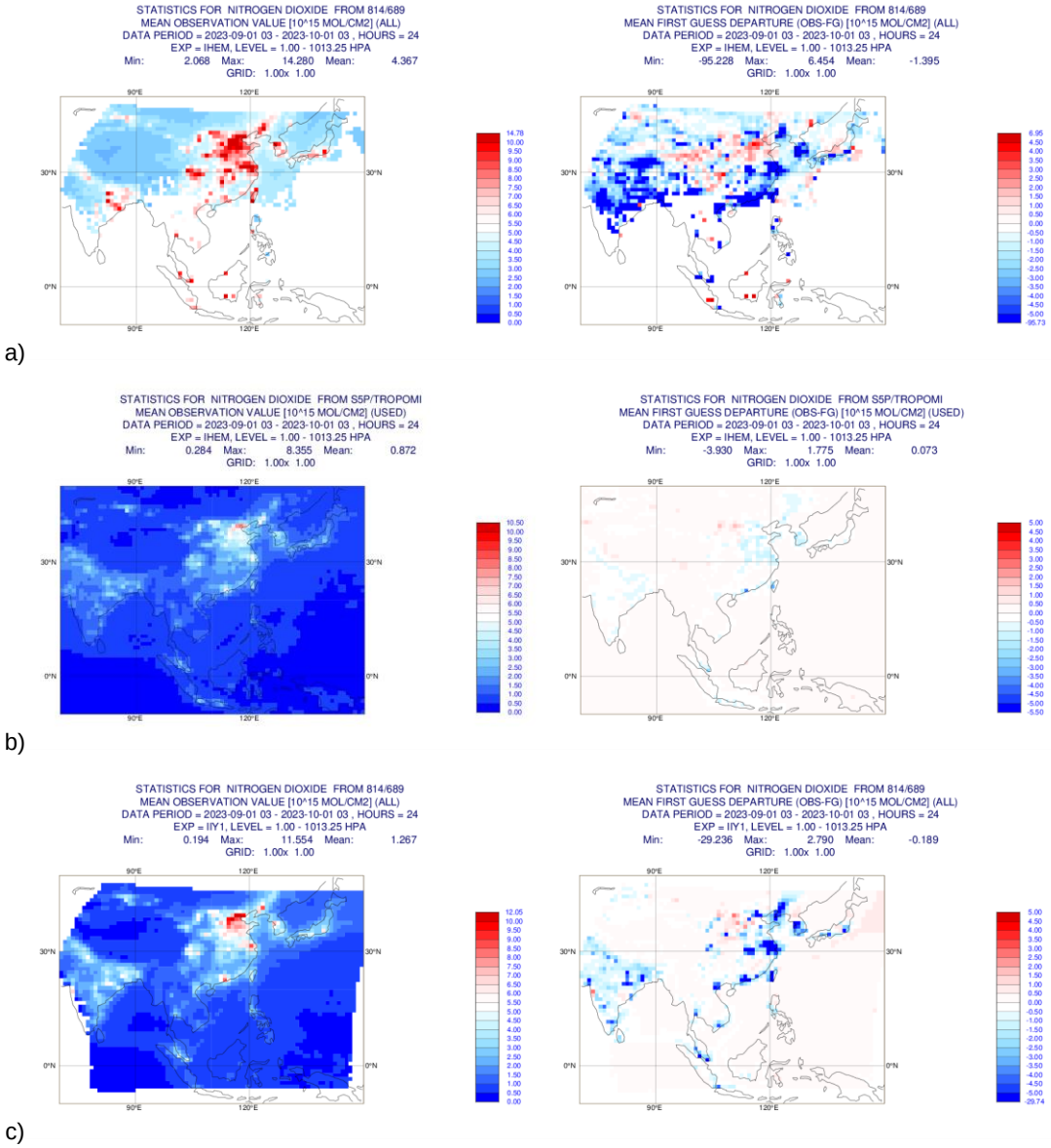

Figure 10: Observation statistics for NRT GEMS (a), TROPOMI (b) and IUP-UB GEMS (c) mean NO_2 observations in 10^{15} molec/cm^2(left panels) and first guess departures (right panels). The analysis covers a period of September 2023.

A more detailed study of the NO_2 first guess departures from NRT GEMS, TROPOMI, and IUP-UB GEMS data (Figure 11) reveals notable differences in means, spread, and systematic biases across the datasets. The histogram (Fig. 11a) highlights that the NRT GEMS data has a larger negative mean departure and a much larger spread that the two other datasets. In contrast, TROPOMI and IUP-UB GEMS show mean values closer to zero with narrower distributions, suggesting they are of better quality. The box plot (Fig. 11b) confirms this, with the NRT GEMS data showing a wider range and more outliers, while the TROPOMI and IUP-UB GEMS datasets have more compact distributions and fewer extreme values. These findings suggest that TROPOMI and IUP-UB GEMS are more suitable for assimilation into the IFS model due to their better quality.

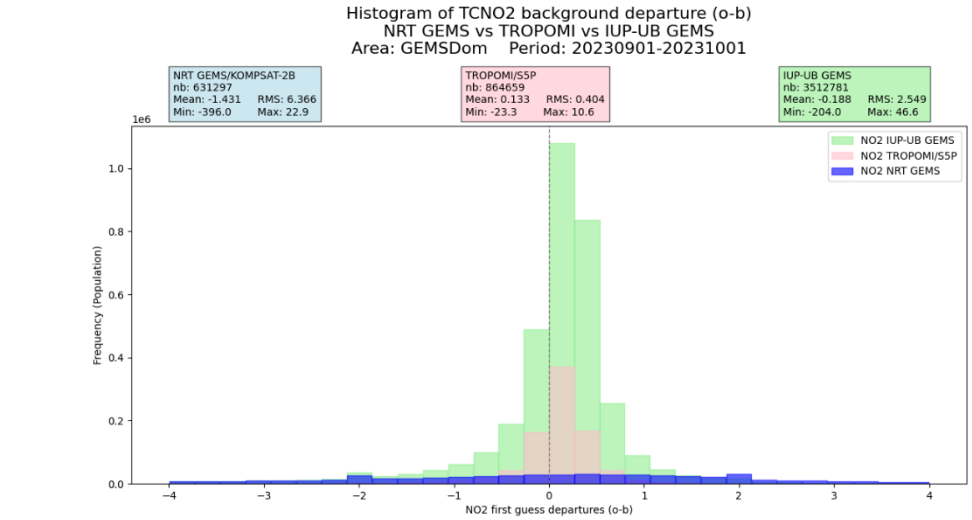

a)

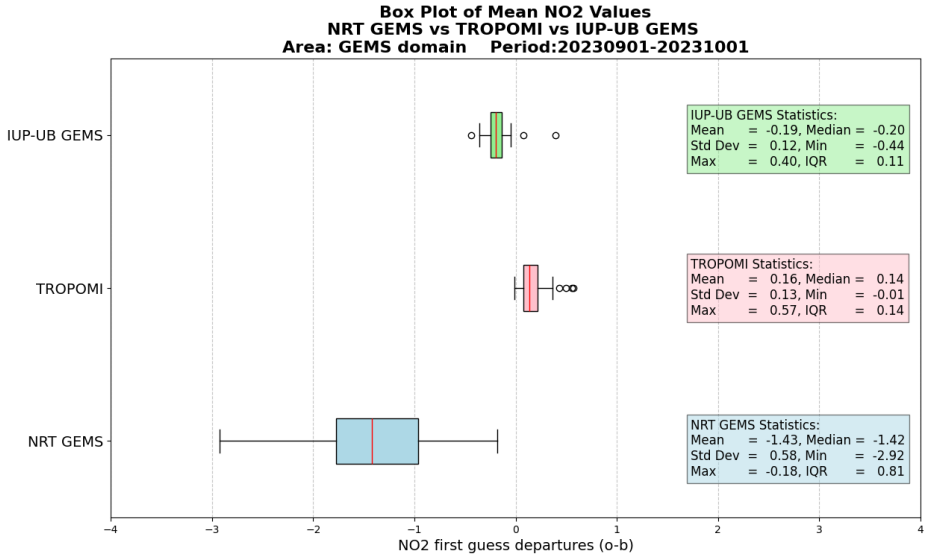

b)

Figure 11: Statistical analysis for the three datasets; NRT NO_2 GEMS, IUP-UB NO_2 GEMS and NO_2 TROPOMI. Upper plot: histogram of the first guess departures, lower plot: box plot of the mean NO_2 values.

Figure 12 illustrates the diurnal cycles of NO_2 tropospheric columns for the IUP-UB GEMS (dark green line) and NRT GEMS (blue line) datasets over the Beijing area, along with their respective IFS first guess diurnal cycles. The IUP-UB GEMS NO_2 data exhibit a typical diurnal pattern, with concentrations peaking in the morning, likely driven by rush-hour traffic and other anthropogenic emissions, and decreasing by mid-day due to active photochemical reactions. The NRT GEMS NO_2 diurnal cycle follows a similar trend but shows systematically higher concentrations compared to the IUP-UB GEMS throughout the day, reflecting a positive bias already discussed in previous sections.

For both datasets, the IFS first guess overestimates NO_2 concentrations relative to the observations, with differences though in the evolution through the day; the first guess for the IUP-UB GEMS NO_2 data (light green line) has a constant bias to the data, whereas the one for NRT GEMS NO_2 (light blue line) has smaller bias in the morning that gets larger after mid-day. It is important to highlight that the differences in the first guess data between the two data sets are a result of the observation operator application, mainly because of the treatment of

averaging kernels and the spatial sampling of the observations. The first guess is calculated at the time and location of the observations. Since the spatial coverage (latitude and longitude) differs between the IUP-UB GEMS and NRT GEMS datasets, the model interpolates to different grid points, resulting in variations in the sampled model fields and hence in the first-guess values. Furthermore, the IUP-UB GEMS dataset does not include averaging kernels, so the first guess is calculated as a simple vertical integral of the model profile. In contrast, the NRT GEMS dataset includes averaging kernels, which are applied in the observation operator, and any potential biases can further affect the calculated first guess.

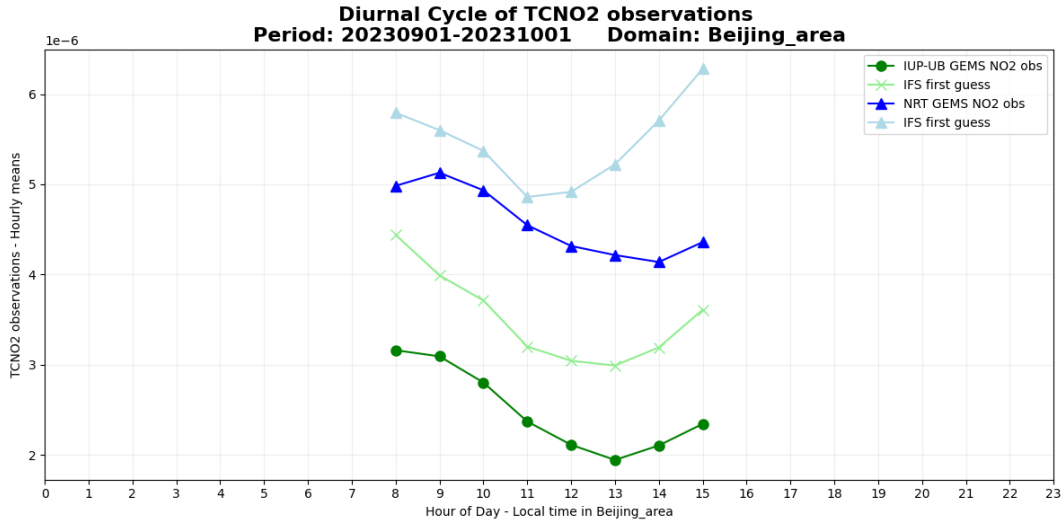

Figure 12: Diurnal cycle of NO_2 observations over Beijing area for IUP-UB GEMS (green) and NRT GEMS (blue) datasets, together with the corresponding IFS first guesses (light green and light blue respectively), in local time.

Next the evaluation of the diurnal cycles of NO_2 tropospheric columns over different regions within the GEMS domain are presented (Figure 13). Urban areas, such as Korea (Fig. 13a) and Beijing (Fig. 12), exhibit pronounced diurnal cycles in NO_2 concentrations, as captured by the IUP-UB GEMS observations, emphasizing the strong impact of human activities. In contrast, rural and sparsely populated regions, such as Tibet (Fig. 13b), show comparatively low NO_2 levels and minimal diurnal variation, with the IFS first guess closely aligning with the observations.

However, across all domains, the IFS first guess systematically overestimates NO_2 concentrations, suggesting potential biases in the emissions inventory utilized by the operational IFS. This overestimation may stem from the lack of fine-scale local details in the emissions data. The results highlight the IUP-UB GEMS dataset's capability to accurately capture spatial and temporal variations in NO_2 levels, reinforcing its value as a key resource for air quality monitoring and its potential integration into the CAMS system for assimilation purposes.

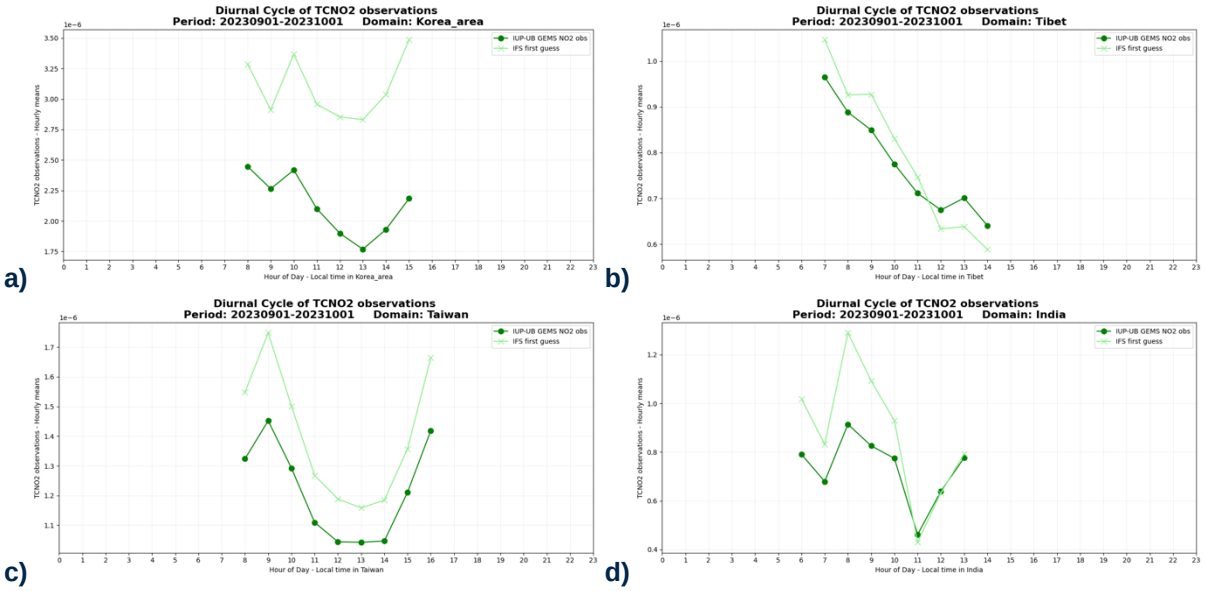

a) **b)** **c)** **d)**

Figure 13: Diurnal cycle of NO_2 observations for IUP-UB GEMS (green) and its IFS first guesses (light green) for different locations within the GEMS domain, in local time; (a) Korea Peninsula, (b) Tibet area, (c) Taiwan, (d) India

The data quality of the IUP-UB GEMS data is deemed good enough to start assimilation tests with the data and their results will be assess in the remainder of the project.

5 Evaluation of GEMS O_3 observations

GEMS measures hourly ozone profiles (O3P) and total column ozone (O3T). This continuous daytime monitoring capability allows GEMS to capture the diurnal cycle of O_3, which is shaped by photochemistry, transport, and emissions. As such, GEMS is a valuable tool for observing total ozone over some of the most densely populated regions on Earth.

Validation studies conducted to date have compared GEMS O_3 data with ground-based observations and satellite products (Garane et al., 2023). These studies report a bias in GEMS O3 data connected with the annual cycle and the latitude. Comparisons with TROPOMI, OMI and GOME O_3 retrievals show on the one hand a very good agreement during NH spring, summer and autumn south of 30°N, but on the other a negative bias northward of 40°N mainly during NH winter.

This observed north-south difference forms an apparent artificial gradient along the latitudinal axis and is a documented issue in the GEMS retrieval algorithm (Baek et al., 2023, 2024). Several retrieval-specific factors can contribute to this feature:

- Geostationary viewing geometry: The fixed position of GEMS results in longer atmospheric path lengths at higher latitudes, potentially amplifying retrieval uncertainties.
- Surface reflectance variability: Differences in surface properties, such as bright, reflective surfaces in the south versus darker, vegetated surfaces in the north, influence retrieval accuracy.
- Aerosol and cloud cover: These factors impact the stratosphere-troposphere separation algorithms, as GEMS relies on ozone-sensitive wavelengths that can be influenced by atmospheric conditions.
- Latitude-dependent retrieval assumptions: Variability in atmospheric composition and environmental conditions along the latitudinal axis further complicates retrieval accuracy.

Despite these challenges, GEMS provides valuable insights into O_3 distribution and dynamics, making it an important asset for air quality and climate monitoring in the CAMS system.

5.1 Near Real time GEMS O_3 total column monitoring

The evaluation methodology for GEMS O_3 follows the same approach as for GEMS NO_2: analysis of the CY49R1 e-suite experiment monitoring GEMS O_3 data over a 12-month period, with comparisons against TROPOMI observations and the IFS model first guess.

To provide an overview of the data sets' coverage and relevance, Figure 14 presents snapshots of total column O_3 daylight measurements over the GEMS domain, comparing data from TROPOMI and GEMS, illustrating the different coverage from the geostationary and polar orbiting satellites. GEMS raw measurements are subject to retrieval's quality control filters, which also lead to some data being excluded. These differences underscore the complementary strengths and limitations of the two datasets in monitoring ozone.

	S5P	GEMS
0Z	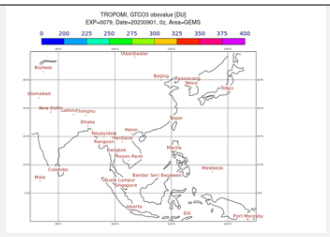	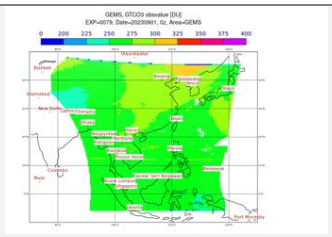
1Z	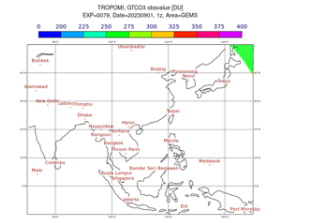	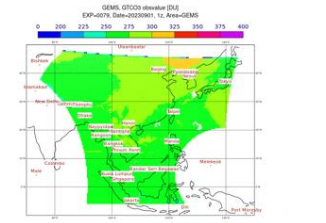
2Z	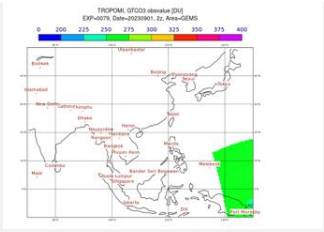	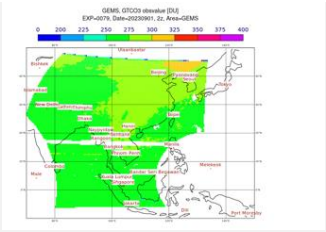
3Z	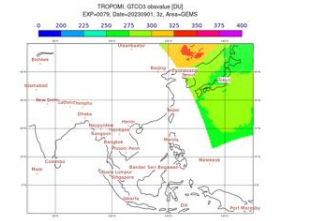	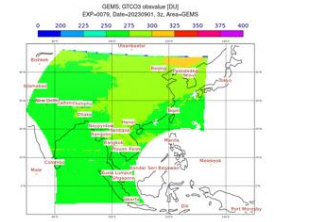
4Z	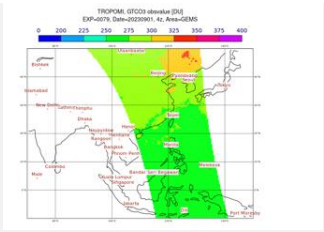	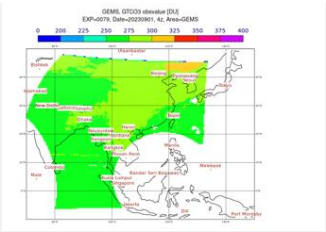
5Z	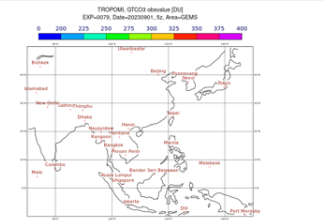	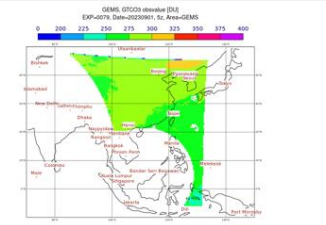
6Z	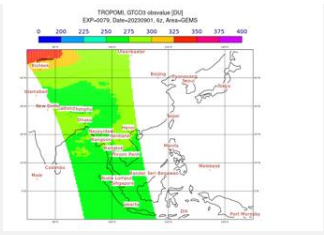	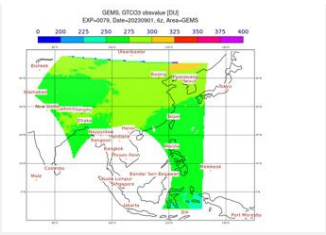

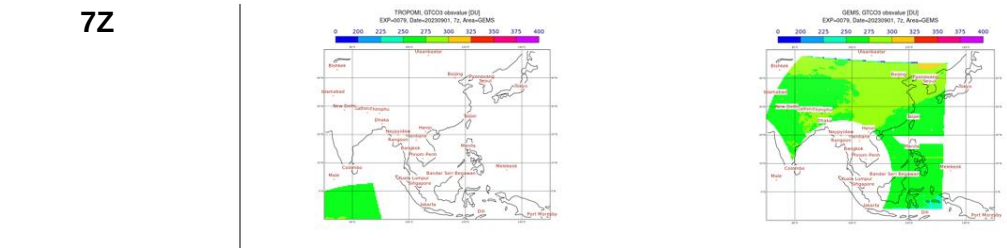

Figure 14: Observation snapshots of TROPOMI (upper row) and GEMS (lower row) O_3 measurements in DU over GEMS domain for 1st September 2023 and different times (2z refers to 02:00 in UTC etc.).

Figure 15 presents the daily-averaged time series of total column ozone from the NRT GEMS observations and TROPOMI observations over the GEMS domain for the period spanning 1st of September 2023 to 1st of September 2024. Both datasets display a consistent seasonal evolution over the course of the year, indicating a general agreement in their ability to capture large scale-variations in ozone levels. Moreover, they reflect a seasonal ozone cycle, with ozone concentrations increasing slightly during the spring months and decreasing toward the late summer and early autumn. This pattern aligns with expected atmospheric ozone dynamics influenced by seasonal variations in photochemistry, transport, and stratosphere-troposphere exchange processes. While the overall evolutions are aligned, TROPOMI observations tend to show slightly higher daily-averaged ozone levels than the NRT GEMS data, a pattern that indicate a systematic bias between the two datasets. This is consistent with known biases where GEMS O_3 has been reported to show lower values in certain conditions compared to TROPOMI (Garane et al., 2023). However, this bias would not be limiting the assimilation of the data as CAMS applies variational bias correction to TCO3 data.

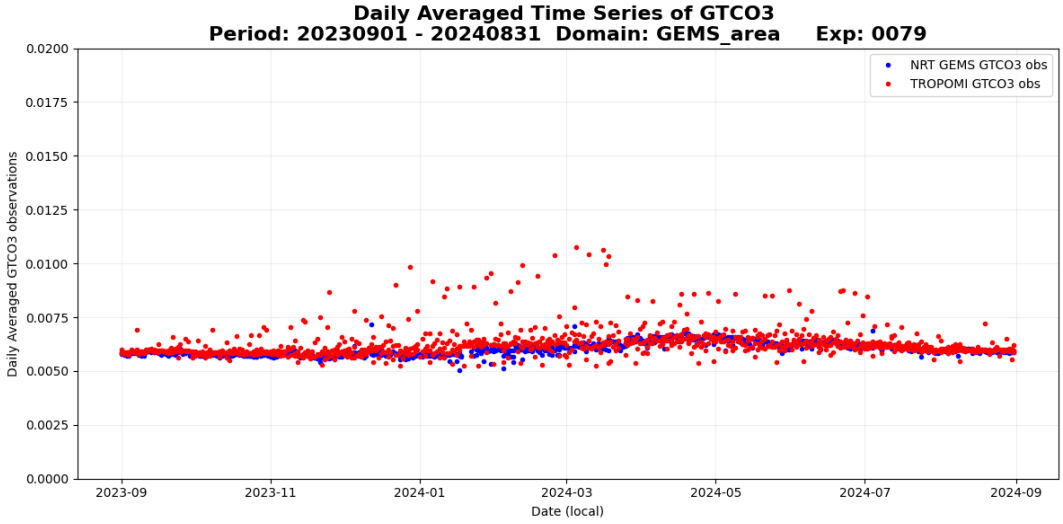

Figure 15: Yearly timeseries of total column ozone as daily averaged values for GEMS (in blue) and TROPOMI (in red) satellites over GEMS domain for 1st September 2023 until 1st of September 2024.

To look at the agreement of GEMS O_3 with the model's first guess, Figure 16 depicts the uncorrected first guess departures for GEMS and TROPOMI O_3 datasets, i.e. the departures calculated before applying the IFS model's bias correction to the data. Both remain relatively close to zero throughout the year suggesting a better consistency to the model for GEMS O_3 in comparison with GEMS NO_2. TROPOMI data generally show smaller departures from the

first guess than GEMS, particularly between November 2023 to March 2024, where GEMS underestimates the total O_3. It can be here emphasized that while the absolute bias between the two datasets is small (on the order of 10^{-4} or less), the relative magnitude becomes more significant when considering the total column ozone values, which fall within the range of 0.005-0.01 molec/cm^2. This bias corresponds to approximately 2.5-5% of the absolute values.

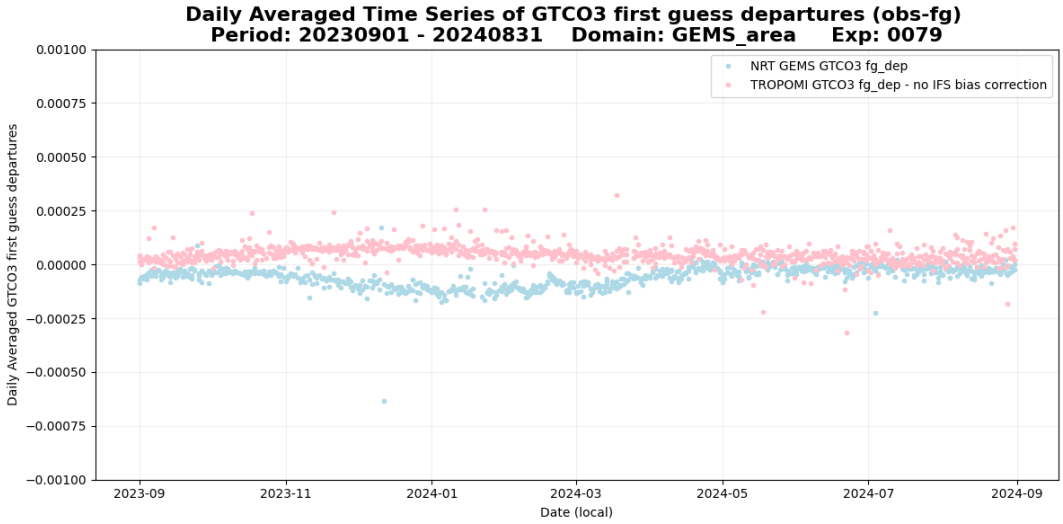

Figure 16: Yearly timeseries of O_3 first guess departures for GEMS (light blue) and TROPOMI (pink) satellites, as daily averaged values. The data cover the whole evaluated period from 1st of September 2023 to 1st of September 2024, over the GEMS domain.

Figure 17 illustrates the same departures of Figure 16 as maps over the GEMS domain for winter and summer months 2024. The winter underestimation increases for higher latitudes, as it is shown by the larger negative (blue) departures in Figure 18a for GEMS O_3. In contrast, this bias is significantly smaller during summer months, reflecting improved alignment with the first guess and TROPOMI at mid and high latitudes (Figure 17c). However, GEMS O_3 has a positive bias in summer over the high-elevation regions of the Tibetan Plateau (Fig.17c). This anomaly suggests retrieval challenges related to the separation of stratospheric and tropospheric ozone contributions in complex topographical regions.

TROPOMI, on the other hand, shows a more stable behaviour across seasons. In summer, it exhibits a small negative bias over tropical regions and oceanic areas, while in winter, a slight positive bias is observed over continental regions. These patterns indicate that TROPOMI maintains a relatively consistent performance, with less pronounced seasonal and spatial variability compared to GEMS O_3. This contrast highlights the need for refinement in GEMS retrieval algorithms, particularly for challenging regions such as high altitudes and northern latitudes.

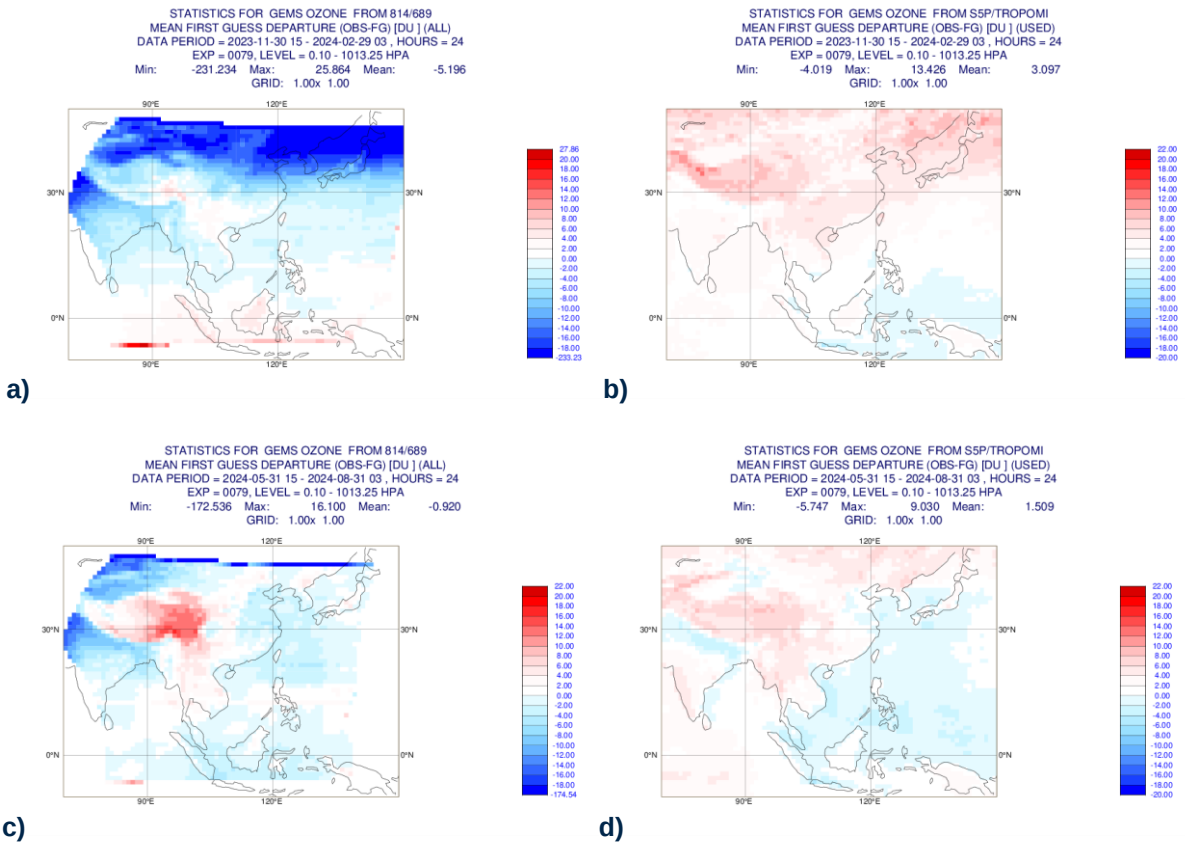

Figure 17: Map plots over GEMS domain of mean first guess departures for GEMS (left panels) and TROPOMI (right panels) satellites, as daily means for NH winter months 01.12.2023-01.29.02.2024 (upper panels) and NH summer 01.06.2024-31.08.2024 (lower panels).

Furthermore, Figures 17a and 17c illustrate the presence of extreme low and high GEMS O_3 values, particularly at the borders of the domain. The GEMS dataset shows a significant higher prevalence of the outliers compared to TROPOMI, as shown in the box plot (Figure 18a). These extremes contribute to the notably larger RMS error for GEMS observations, indicating higher variability and reduced consistency, compared to the relatively stable and consistent TROPOMI observations, which exhibits substantially fewer outliers and lower RMS errors.

In general, the interquartile ranges, overall box sizes and medians between GEMS and TROPOMI datasets are comparable, despite the significant differences in their minimum and maximum values. This fact suggests that excluding the extreme outliers (particularly the anomalously low values in the GEMS dataset), would not lead to a statistically significant bias or compromise the overall analysis. Figure 19b shows the distribution of the two data sets after applying a filtering approach that excludes values beyond the 0.5th and the 99.5th percentiles. The method ensures that the statistics become more robust and less influenced by noise or anomalies caused by extreme values, allowing for a more accurate and reliable comparison. Now the mean and root mean square (RMS) error values of GEMS and TROPOMI align closely, indicating negligible bias between them. Such alignment is consistent with expectations for the upcoming version 3 of the GEMS retrieval algorithm (K. Lee et al., 2024), which is anticipated to further reduce the known biases of GEMS measurements.

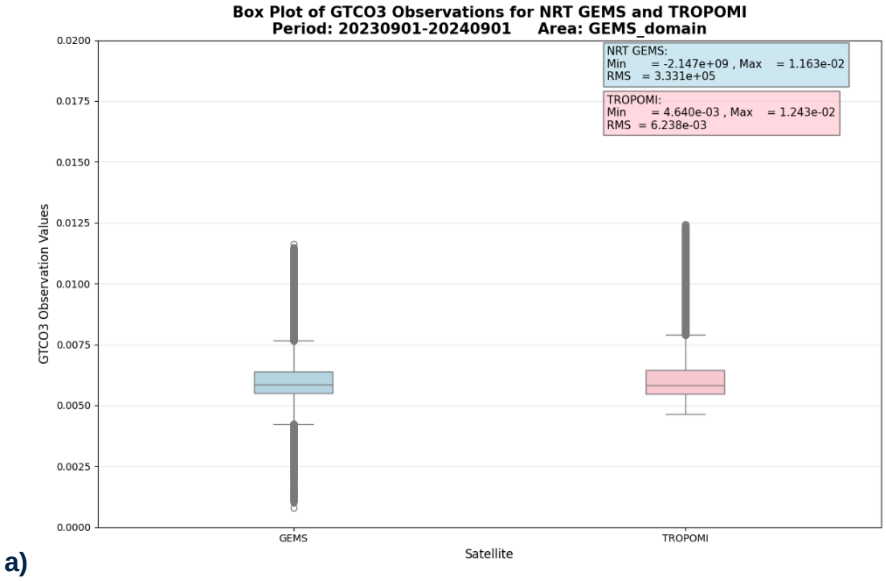

a)

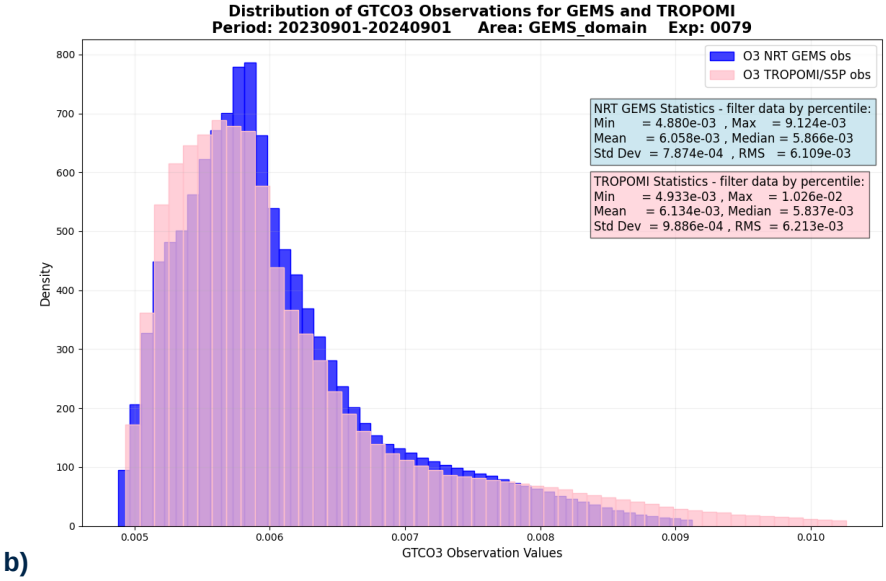

b)

Figure 18: Statistical analysis for the GEMS and TROPOMI ozone datasets; box plot (a) and histogram (b) of O_3 measurements. The histogram does not include the extreme outliers.

The existence of extreme observation values in GEMS measurements at the domain boundaries is clearly depicted also in the following scatter plots. Figure 19 shows a series of scatter plots of GEMS and TROPOMI O_3 total column data, for the whole examined 12 months period over the GEMS domain. The scatter plots of observations over latitude (Fig. 19a and 19b) verify that TROPOMI in contrast to GEMS does not have such extreme first-guess departures and that the data show less variability. GEMS's large negative first-guess departures in northern latitudes and large positive departures at southern latitudes are visible. Moreover, the biases in the latitudinal distribution are highlighted; the total column values of GEMS observations tend to increase north of 30°N, with a noticeable bulge in the number of observations around these latitudes – a fact that has great influence on the first guess departures in northern GEMS domain (Fig. 19c and 19d).

While both datasets perform well under high solar elevation conditions (Fig. 19e and 19f), the GEMS retrievals demonstrate greater sensitivity under lower sunlight conditions (SOE<30°), with larger biases and higher density of outliers. To address these issues in the CAMS analysis

and reduce the retrieval noise (at least until retrieval algorithm enhancements), blacklisting the observed data lower to 30° SOE would be considered.

Finally, as far as the cloud parameters is concerned, distinct differences between TROPOMI and GEMS data is identified. For cloud top pressure, TROPOMI first guess departures remain consistently centred around zero across all pressure ranges (Fig. 19g), indicating minimal sensitivity to cloud top variations. In contrast, GEMS data (Fig. 19f) show higher variability, with notably larger departures at lower cloud top pressures (<500 hPa), suggesting an increased influence of higher clouds on the GEMS observations. Similarly, when assessing cloud cover, TROPOMI first guess departures (Fig. 19i) exhibit a stable and uniform pattern across the entire cloud cover spectrum, whereas GEMS data (Fig. 19h) display greater variability at low cloud cover percentages (<30%). However, GEMS first guess departures stabilize and align with TROPOMI at higher cloud cover values (>50%), demonstrating improved reliability under moderate to high cloud conditions.

These findings suggest that, while TROPOMI data perform robustly across varying cloud parameters, GEMS observations may benefit from further evaluation and possible exclusion of data under specific conditions, such as low cloud cover and low cloud top pressure.

	NRT GEMS TC O_3	**TROPOMI TC O_3**
Obs vs Lat	a) 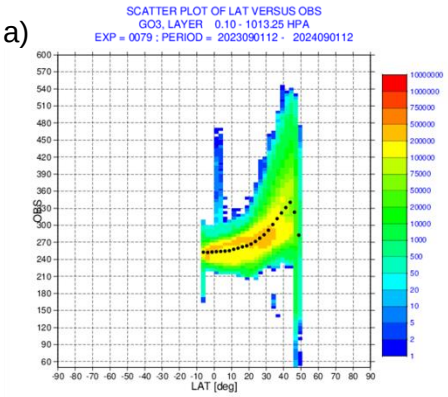	b) 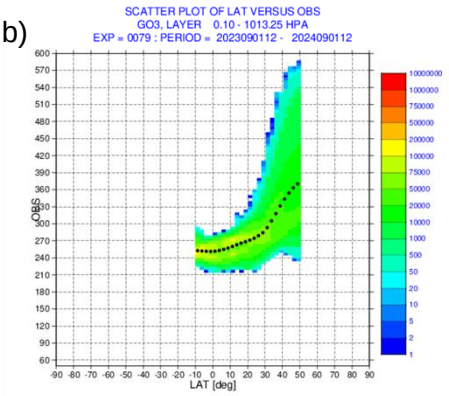
Fg_dep vs Lat	c) 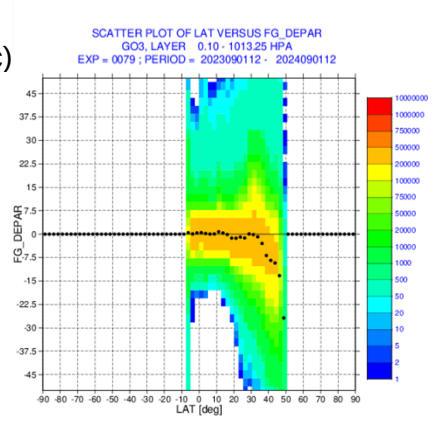	d) 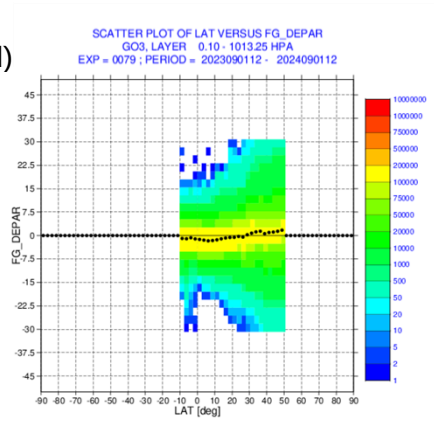

Fg_dep vs Solar Elevation

Fg_dep vs cloud top pressure

Fg_dep vs Cloud cover

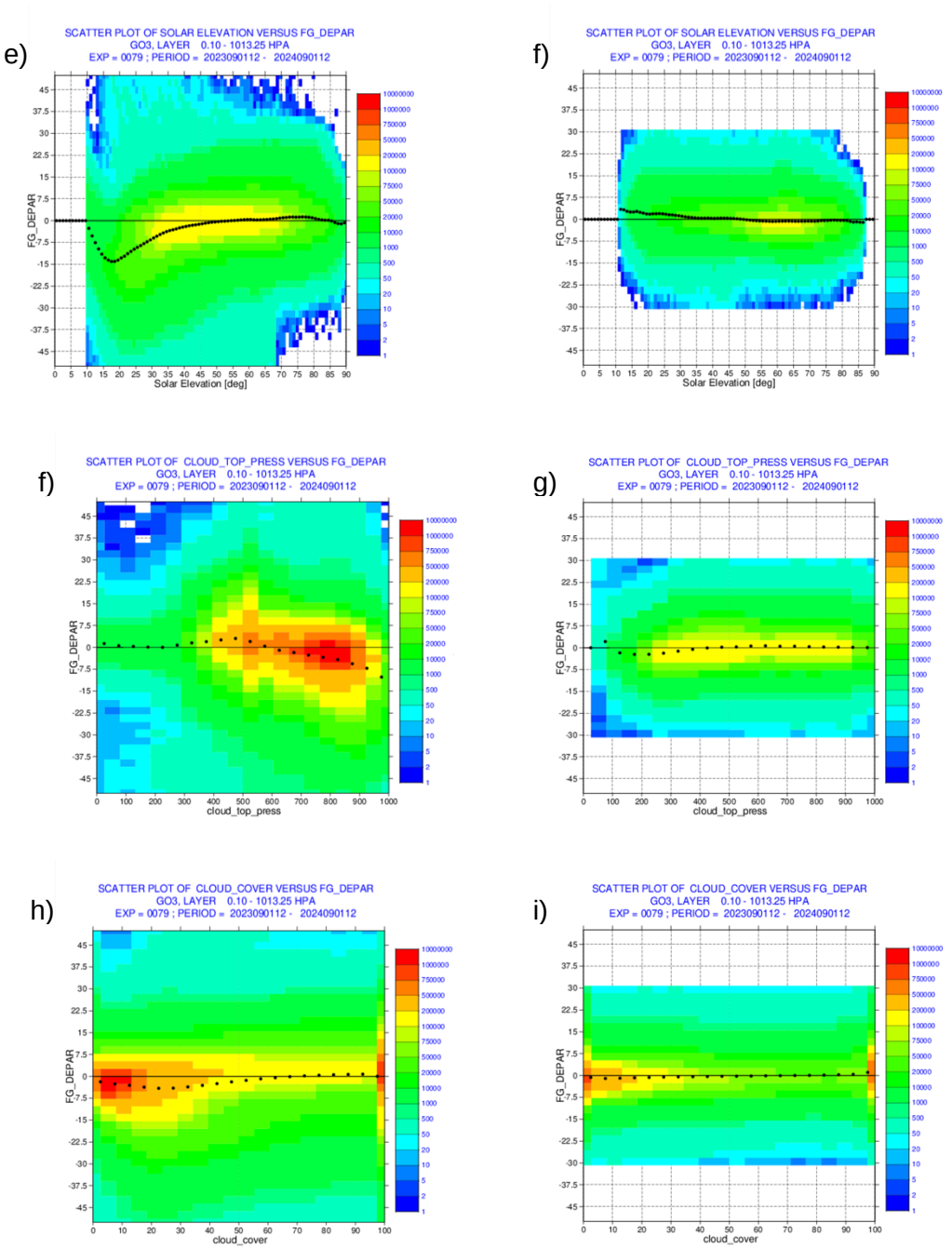

Figure 19: Scatter plots for GEMS (left panels) and TROPOMI (right panels) total column O_3 data; observation and first guess in comparison with latitude, solar elevation and cloud cover give an overview of the biases between the 2 datasets and the CAMS system Note: difference in yaxis scale for the two datasets.

Figure 20 illustrates the seasonal mean diurnal cycle over Beijing area for GEMS O_3 observations in local time, after the aforementioned filtering of the outliers, and the IFS first guess. The diurnal cycles capture the underestimation of GEMS O_3 in DJF, compared with the predicted levels from IFS. There is in general a good agreement of GEMS O_3 levels and IFS first guess, especially in JJA, indicating the ability of GEMS to effectively capture O_3 variations under optimal conditions.

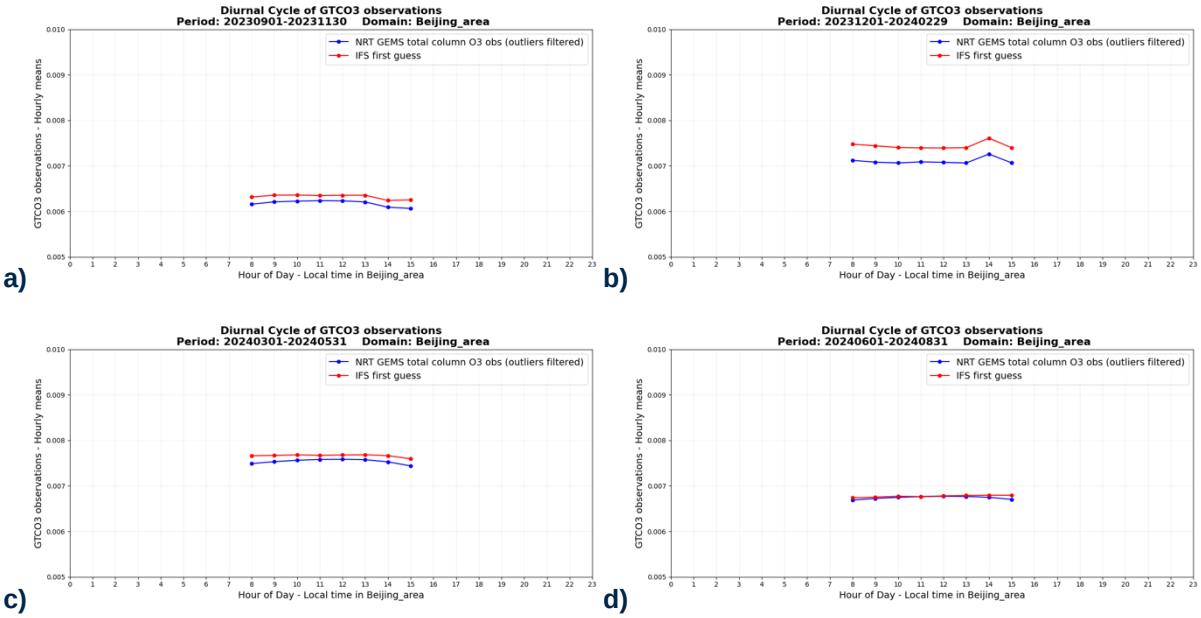

Figure 20: Seasonal mean diurnal cycle of O_3 GEMS observations (blue) and the IFS first guess (red) over extended Beijing area, in local time, by season: (a) SON 2023, (b) DJF 2024, (c) MAM 2024 and (d) JJA 2024.

The GEMS O_3 monitoring highlights that while challenges remain, the GEMS O_3 dataset is suitable for assimilation tests with the IFS, if these large outliers are not used. The IFS applies a variational bias correction mechanism to total column ozone data that should be able to deal with some of the systematic discrepancies during the assimilation process. Furthermore, variational quality control and first-guess checks are applied to the data, which currently removes all ozone data with first-guess departures greater than 30 DU.

5.2 Near Real time GEMS O_3 total column assimilation

Analysing the impact of GEMS O_3 measurements on CAMS forecasts and analyses, an IFS experiment was set up (Table 2) to assimilate the GEMS data for the first time. The assessment consists of two main components: a six-month evaluation of GEMS O_3 and an analysis of its impact on CAMS forecasts by comparing with independent observations.

Firstly, the outcome of the six-month experiment of GEMS O_3 assimilation is discussed. Figure 21a shows the daily averaged timeseries of GEMS O_3 observations and their equivalent model first guess and analysis over GEMS domain. Figure 21b shows histograms of the distribution of the first guess departures and the analysis departures for GEMS O_3 and TROPOMI O_3. The GEMS O_3 observations exhibit a consistent temporal evolution, with seasonal variability, without extreme low or high values, as these extremes are rejected by the model's quality controls. As far as the departure statistics of the used data in the assimilation process is concerned, GEMS and TROPOMI have a similar behaviour, with both analysis departures following a Gaussian distribution centred close to zero. The standard deviation and RMS error are very close for the two satellites; both have achieved a RMSE reduction for the analysis of more than 25%. Small differences with lower GEMS analysis standard deviation than TROPOMI could be due to the abundant amount of GEMS data during daylight.

a)

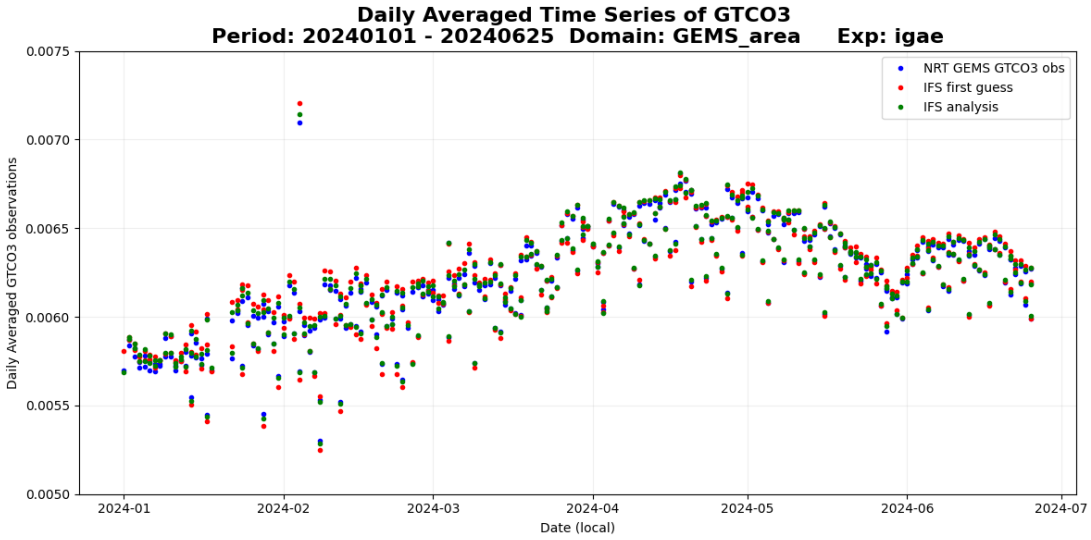

b)

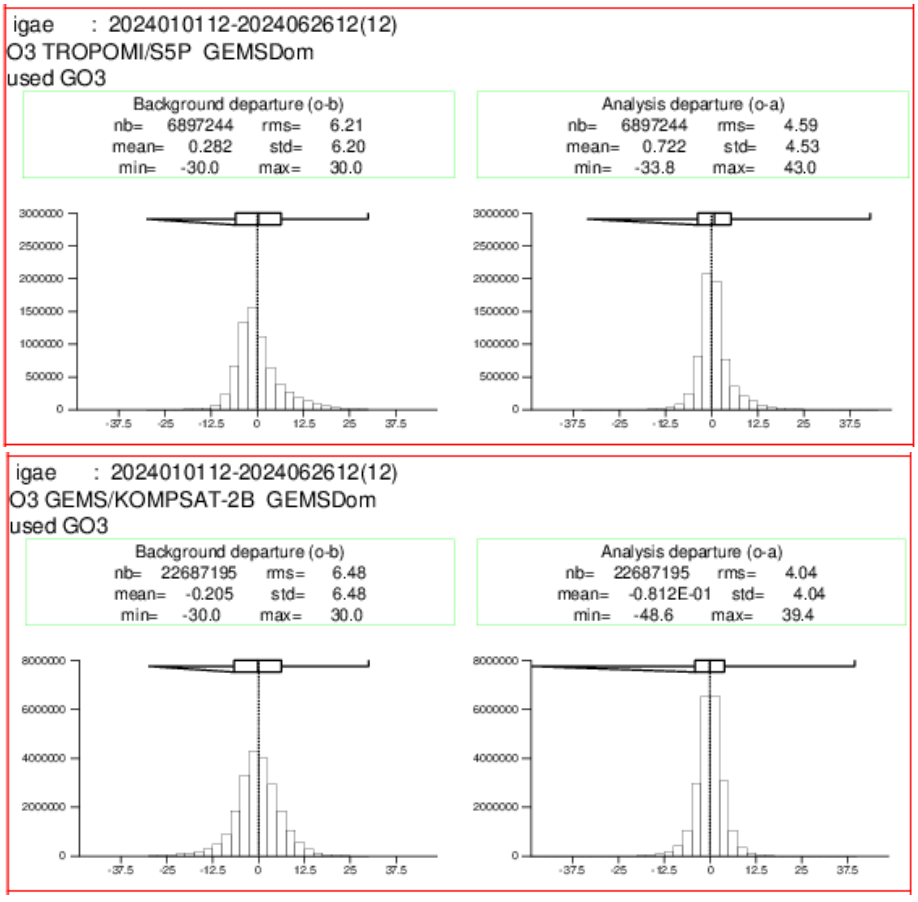

Figure 21: Evaluation for the period 1st of January 2024 to 25th of June 2024 over the GEMS domain. (a) Timeseries of GEMS O_3 as daily averaged values for GEMS observations (blue) and their equivalent first guess (red) and analysis (green) as calculated by IFS. (b) Distribution of first guess departures (left panels) and analysis departures (right panels) of GEMS and TROPOMI O_3 data.

Figure 22 show maps of the analysis departures for GEMS and TROPOMI O_3 observations over the entire GEMS domain (22a and 22b) and the Beijing region (22c and 22d). For GEMS observations, the analysis departures exhibit a smooth pattern, reinforcing the systematic underestimation of GEMS O_3 values. The mean analysis departure for GEMS across the domain is slightly negative, with a mean of approximately -3.1 DU. Larger departures are concentrated in northern latitudes and over oceanic areas, together with extreme negative

departures in certain grid cells; likely linked to retrieval challenges discussed previously and lower data coverage in these regions. Over the Beijing region, GEMS analysis departures are consistently negative with small variations, reflecting the high temporal and spatial resolution of the dataset and its ability to capture diurnal ozone evolution in densely populated and highly dynamic areas.

In contrast, TROPOMI analysis departures are predominantly positive, with a mean positive bias of 6.3DU and more pronounced over crowded urban areas. This could suggest that the assimilation of high-resolution GEMS data, with its superior temporal and spatial coverage, could provide significant added value for improving the representation of ozone dynamics in such complex regions.

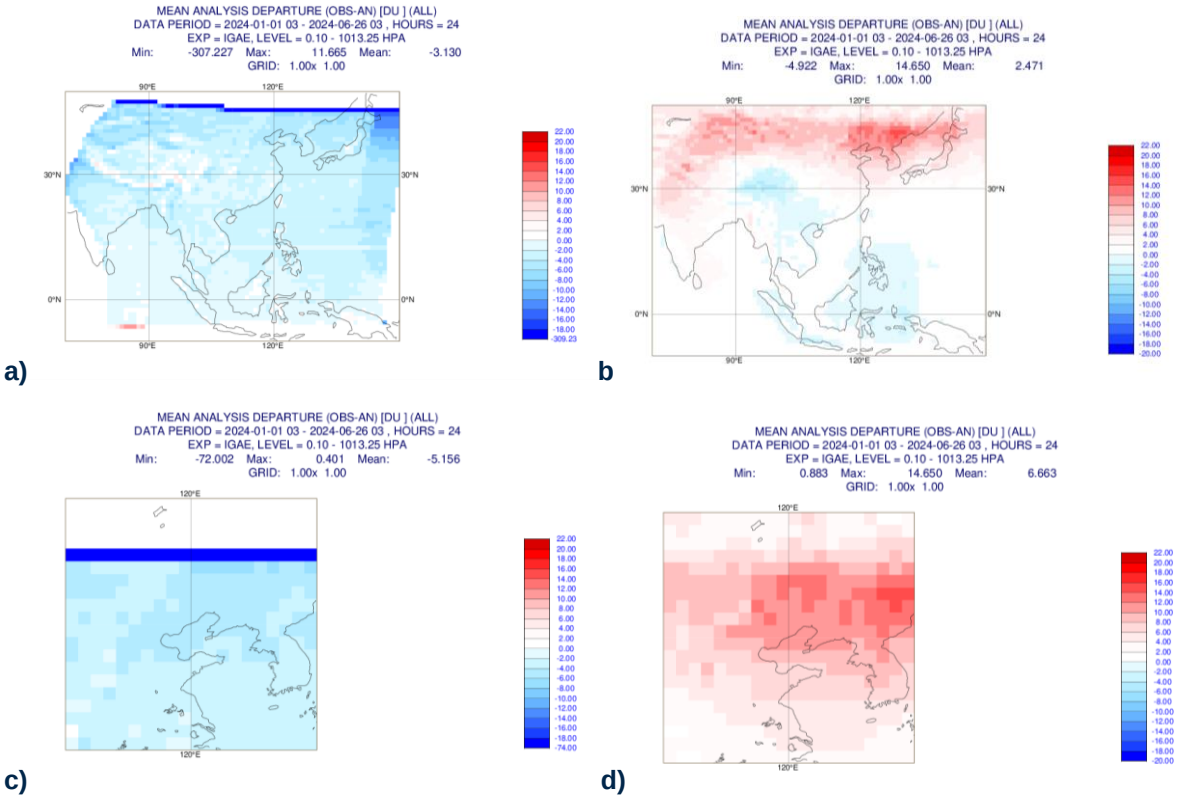

Figure 22: Maps of analysis departures of GEMS (left panels) and TROPOMI (right panels) total column O_3 observations, over the GEMS domain (a,b) and the extended Beijing domain (c,d).

The scatter plots of Figure 23 demonstrate the overall effectiveness of the assimilation process for GEMS O_3 measurements. The first guess departures of Fig. 23a shows significant variability in departures across latitudes. The analysis departure scatter plot though reveals that the analysis effectively reduces the variability in departures across all latitudes. Despite overall improvement, the northern mid-latitudes (30°N–50°N) and southern high-latitudes (30°S–40°S) continue to exhibit slightly higher departures in the analysis stage – underlining the necessity of the improvement of retrieval issues for any further operational use of the geostationary satellite data.

	NRT GEMS TC O_3	TROPOMI TC O_3
Fg_dep vs Lat	a) 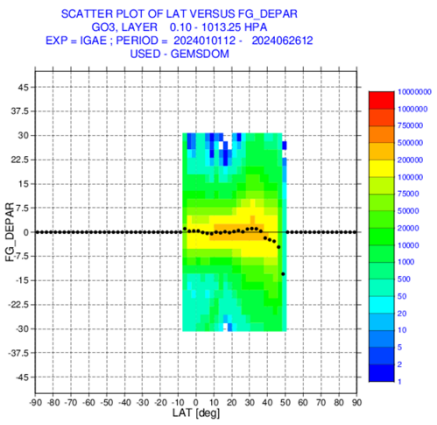	b) 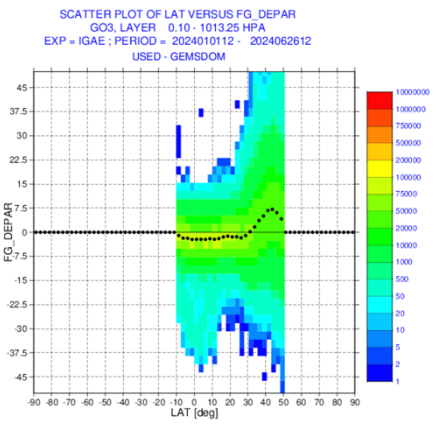
Ana_dep vs Lat	c) 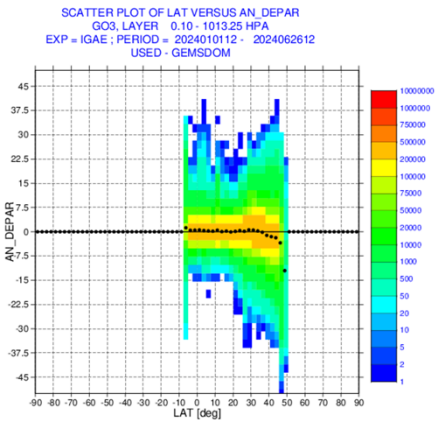	d) 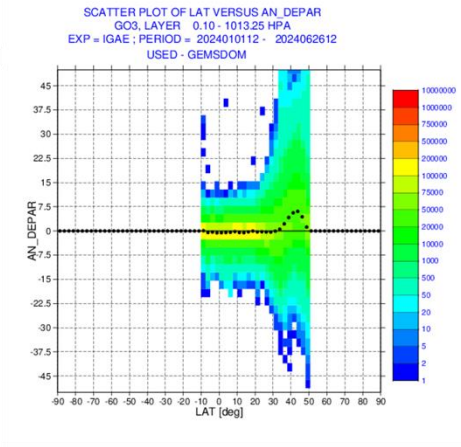

Figure 23: Scatter plots of first guess (a,b) and analysis (c,d) departures in correlation with latitude for NRT GEMS O_3 (left panels) data and TROPOMI (right), for the assimilated period, over the GEMS domain.

To evaluate the impact of GEMS O_3 assimilation within CAMS, comparisons are made between the experiment that assimilates GEMS O_3 data and the reference one, where GEMS data were only monitored but not assimilated. Figure 24 illustrates the differences of GEMS O_3 assimilation-minus-reference in total column ozone ($GTCO_3$ in Fig.24a) and surface ozone (SFC GO_3 in Fig.24b). The assimilation of GEMS O_3 reveals a regionally dependent and systematic influence on ozone concentrations. For total column ozone, the assimilation introduces a distinct latitudinal gradient, with decreases over northern regions (e.g., Korea and Japan) and increases over equatorial regions. These patterns reflect GEMS's measurement characteristics, which capture lower O_3 levels in northern latitudes and higher concentrations nearer the equator. For surface ozone though the impact is small. Over densely populated northern areas, such as Beijing, Seoul, and Tokyo, surface ozone levels decrease, likely influenced by GEMS's lower measurements in these regions. In contrast, increases in surface ozone concentrations are observed over the Indo-China Peninsula and maritime Southeast Asia.

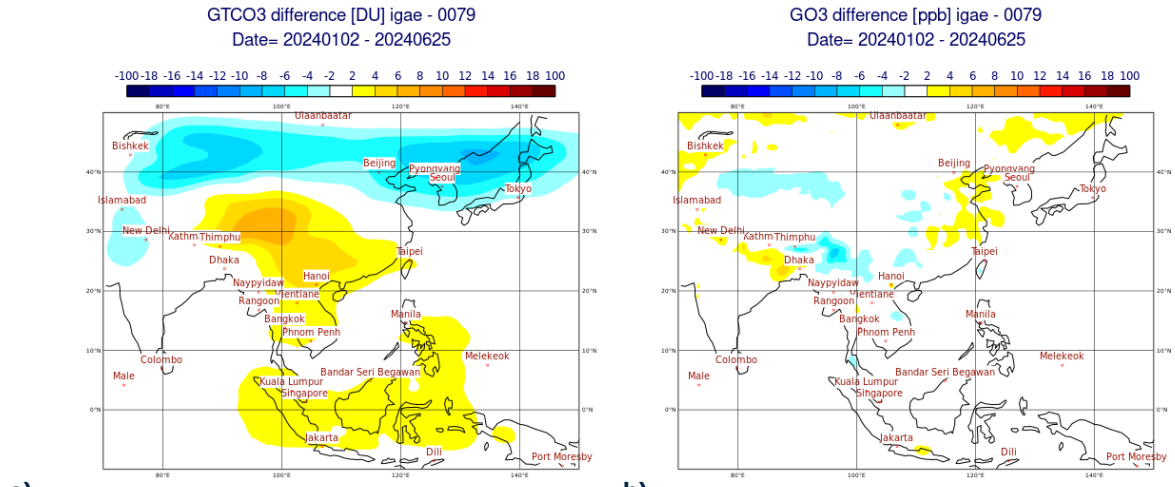

a) b)

Figure 24: Map plots of the differences between the GEMS O_3 assimilation experiment and the reference CAMS o-suite, from 1st January 2024 to 25th June 2024, over GEMS domain.

Further, to evaluate the impact of the analysis on first guess, the analysis increments are shown in Figure 25. The increments quantify the adjustments made by the assimilation process to the model's first guess to produce the final analysis fields. For total column ozone (Figure 25a), positive increments dominate over equatorial regions and along coastlines, while negative increments are concentrated in northern latitudes, including urban areas like Beijing and Seoul. This pattern reflects the systematic low bias in GEMS data over northern regions and a higher bias closer to the equator, as discussed previously. The quality control will remove some outliers but still a significant amount of biased data will pass in the assimilation process (for instance, data with small discrepancy from the control thresholds). For surface ozone, Figure 25b shows a more complex pattern of analysis increments. Negative increments dominate over urban areas, correcting potential overestimations in the first guess fields. Conversely, positive increments are observed over industrial and high populated areas, like Beijing, Shanghai and Tianjin port. This reflects the ability of GEMS data to enhance the representation of O_3, particularly in regions with complex emissions and atmospheric dynamics.

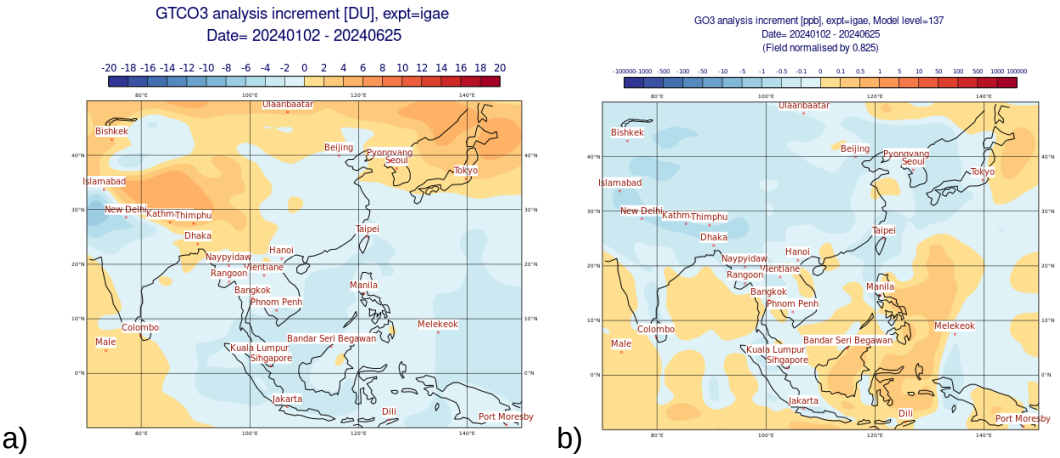

a) b)

Figure 25: Map plots of analysis increments over GEMS domain for the GEMS O_3 assimilation experiment, from 1st January 2024 to 25th June 2024;for total column ozone (a) and for surface ozone (b).

The impact of the geostationary data assimilation is also assessed by comparing with vertical profiles of independent ozone sonde observations which were not assimilated into the system. Figure 26 shows monthly averaged relative O_3 profile differences between the analyses and observations over the GEMS domain for the study period (selection of 4 months). Overall, the inclusion of GEMS data leads to improvements in the representation of ozone across vertical profiles, particularly in lower troposphere and near the surface. For instance, in January 2024 the averaged differences between GEMS O_3 assimilation and the reference experiment show small variations in the upper troposphere and stratosphere (above ~100hPa), with GEMS assimilation aligning closely with the observations. In the lower troposphere, GEMS assimilation leads to reduced positive bias compared to the o-suite, particularly below 500 hPa. These patterns could reflect the capacity of GEMS O_3 data to improve the lower troposphere ozone field, especially in polluted regions, as it is illustrated in Figure 27 for local sites in Hong Kong, China, (27a) and Tsukuba, Japan (27b).

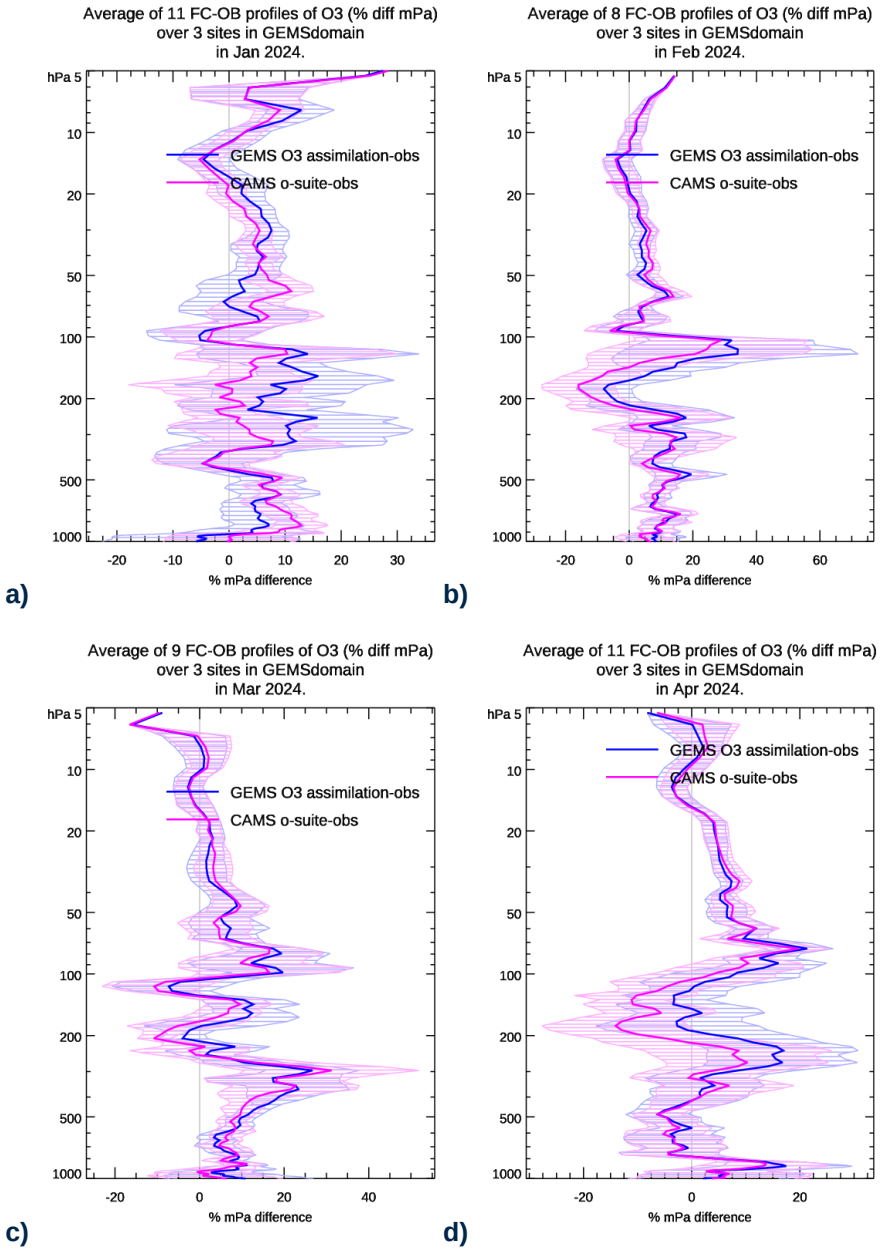

Figure 26: Averaged O_3 profiles for 3 sites in GEMS domain during 4 months of the evaluated period; differences between forecasts from GEMS O_3 (blue) assimilation and CAMS o-suite (pink) with the independent observations of the sites

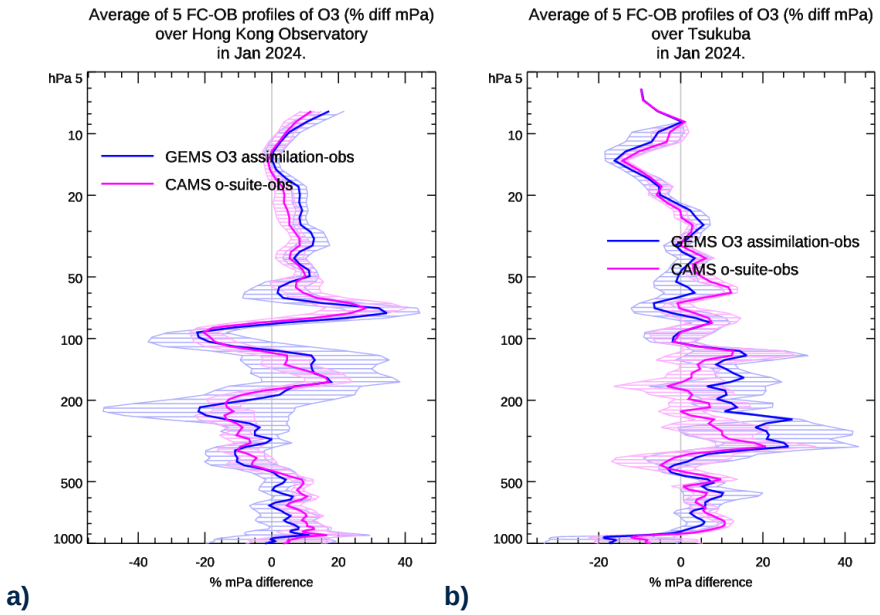

a) **b)**

Figure 27: O_3 profiles for the Hong Kong Observatory in China (a) and the Tsukuba site in Japan (b) during the evaluated period; differences between forecasts form GEMS O_3 assimilation (blue) and CAMS o-suite (pink) and the independent observations of the sites.

The validation of the performance of GEMS O_3 assimilation is studied by comparison with independent surface ozone observations from the air quality monitoring network across China (Figure 28). Here the forecast-minus-observation bias, as well as the root mean square metrics are calculated for different regions of the network and a selection of timeseries for the six-months-evaluation period is presented. In Figure 27a and 27b the results of the comparison with 1.677 stations over whole China show small but consistent improvements for the GEMS O_3 assimilation, with quite stable RMS. Particularly during February and March an enhanced alignment with the independent observations is noted, together with slight reductions in RMS. Looking further at the specific region of Wuhan, the most populated city in central China, the results align with the national trends but show more localized dynamics (Fig. 27c and 27d). Whereas, for the less densely populated Manchuria region which has higher elevation (Fig.27e and 27f), the assimilation of GEMS O_3 is dominated by the positive bias of the observations in spring and early summer, leading to higher RMS.

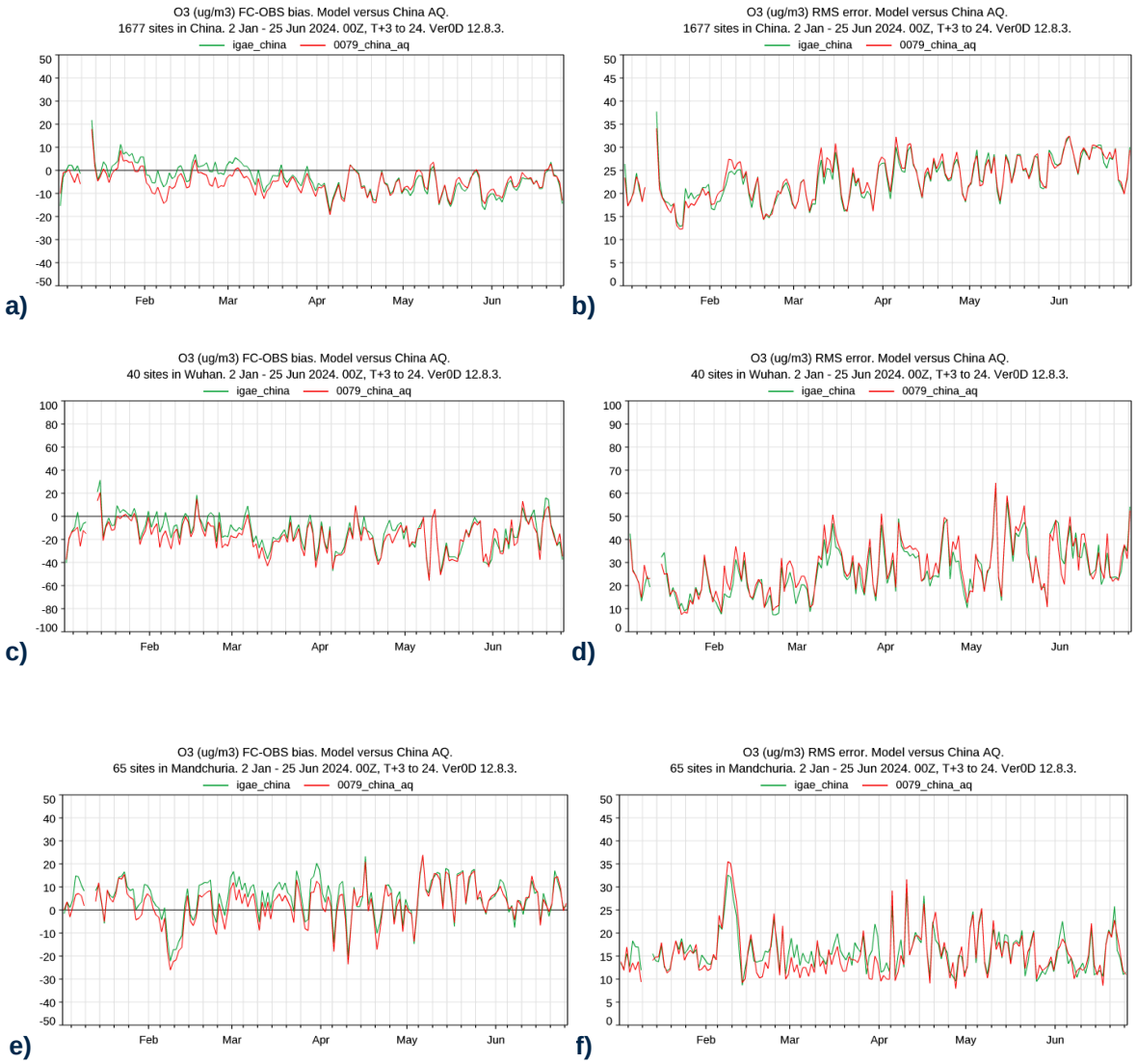

Figure 28: Daily averaged timeseries plots of forecast-minus-observations biases (left panels) and the equivalent RMS errors (right panels). In green the simulation with GEMS O_3 assimilation, and red the reference experiment.

In conclusion, unlike GEMS NO_2 observations, GEMS O_3 observations can be assimilated effectively despite exhibiting a consistent negative bias. The evaluation of the assimilation demonstrates the significant potential of geostationary GEMS O_3 data to enhance the model's ability to represent and forecast ozone concentrations both dynamically and spatially. Ongoing work focuses on deeper analysis and further validation in respect to the impact of GEMS data on CAMS analysis.

6 Conclusion

In this document we have set out for the first time an analysis of the operational geostationary GEMS L2 v.2 NO_2 and O_3 data within the CAMS framework, providing valuable insight into the potential and limitations of GEMS observations for atmospheric composition monitoring.

Initially, the integration of GEMS NRT observations into the operational IFS cycle CY49R1 has been successfully achieved, with continuous monitoring of NO_2 and O_3 data by CAMS.

The evaluation focused on comparing GEMS data with TROPOMI data and model outputs, as well as investigating their impact on model forecasts and analyses. A year-long monitoring experiment was conducted, during which GEMS NO_2 and O_3 were monitored.

The evaluation of the operational GEMS NO_2 version 2 data revealed consistent high biases across much of the domain and strong negative biases along coastlines and the northern part of the domain when compared with TROPOMI and the model. These biases are primarily related to retrieval characteristics, which the upcoming GEMS retrieval algorithm (version 3) aims to address. Despite these limitations, the high temporal and spatial resolution of GEMS NO_2 data offers unique insights into diurnal cycles, particularly over polluted regions and megacities. These data capture significant temporal variations, such as morning rush hour peaks and evening lows, as well as the seasonal variability. However, due to the magnitude of the biases, the operational GEMS NO_2 L2 v2 data are currently unsuitable for direct assimilation into CAMS.

To address these challenges, a collaboration with the University of Bremen (IUP-UB) has been initiated. The IUP-UB GEMS NO_2 retrieval demonstrates improved characteristics, with a stable low bias and closer agreement with TROPOMI data and the model. As a result, the IUP-UB retrieval is being explored for assimilation, with ongoing work expected to continue for the remainder of the project period.

In contrast, GEMS O_3 L2 v2 data exhibit fewer limitations and appear more suitable for assimilation, despite biases associated with the retrieval algorithm and its latitude, ground characteristics, and stratosphere-troposphere separation processes. A six-month assimilation experiment was conducted to evaluate the impact of GEMS O_3 data. The results are promising, with GEMS O_3 analysis comparable to TROPOMI, demonstrating improvements in standard deviation and RMS error. Validations by independent observations shows that GEMS O_3 assimilation enhances sensitivity to local temporal variations, particularly over polluted regions, capturing high-frequency changes effectively.

While challenges persist, including biases and outliers in the retrievals, GEMS observations have demonstrated significant potential to enhance air quality monitoring and atmospheric research. The upcoming version 3 of the GEMS retrieval algorithm is expected to further mitigate current limitations. Furthermore, the joint assimilation of polar-orbiting satellites like TROPOMI and geostationary observations from GEMS shows strong potential for complementing their respective strengths. This synergistic approach could significantly advance the representation of atmospheric composition and improve air quality forecasting in dynamic and diverse environments.

7 References

Baek, K., Bak, J., Kim, J. H., Park, S. S., Haffner, D. P., & Lee, W. (2024). Validation of geostationary environment monitoring spectrometer (GEMS), TROPOspheric Monitoring Instrument (TROPOMI), and Ozone Mapping and Profiler Suite Nadir Mapper (OMPS) using pandora measurements during GEMS Map of Air Pollution (GMAP) field campaign. *Atmospheric Environment*, *324*, 120408. https://doi.org/10.1016/j.atmosenv.2024.120408

Baek, K., Kim, J. H., Bak, J., Haffner, D. P., Kang, M., & Hong, H. (2023). Evaluation of total ozone measurements from Geostationary Environmental Monitoring Spectrometer (GEMS). *Atmospheric Measurement Techniques*, *16*(22), 5461–5478. https://doi.org/10.5194/amt-16-5461-2023

Bak, J., Baek, K.-H., Kim, J.-H., Liu, X., Kim, J., & Chance, K. (2019). Cross-evaluation of GEMS tropospheric ozone retrieval performance using OMI data and the use of an ozonesonde dataset over East Asia for validation. *Atmospheric Measurement Techniques*, *12*(9), 5201–5215. https://doi.org/10.5194/amt-12-5201-2019

Bak, J., Kim, J. H., Liu, X., Chance, K., & Kim, J. (2013). Evaluation of ozone profile and tropospheric ozone retrievals from GEMS and OMI spectra. *Atmospheric Measurement Techniques*, *6*(2), 239–249. https://doi.org/10.5194/amt-6-239-2013

Beirle, S., Hörmann, C., Jöckel, P., Liu, S., Penning de Vries, M., Pozzer, A., Sihler, H., Valks, P., & Wagner, T. (2016). The STRatospheric Estimation Algorithm from Mainz (STREAM): estimating stratospheric NO2 from nadir-viewing satellites by weighted convolution. *Atmospheric Measurement Techniques*, *9*(7), 2753–2779. https://doi.org/10.5194/amt-9-2753-2016

Boersma, K. F., Eskes, H. J., & Brinksma, E. J. (2004). Error analysis for tropospheric NO2 retrieval from space. *Journal of Geophysical Research: Atmospheres*, *109*(D4). https://doi.org/10.1029/2003JD003962

Bucsela, E. J., Krotkov, N. A., Celarier, E. A., Lamsal, L. N., Swartz, W. H., Bhartia, P. K., Boersma, K. F., Veefkind, J. P., Gleason, J. F., & Pickering, K. E. (2013). A new stratospheric and tropospheric NO2 algorithm for nadir-viewing satellite instruments: applications to OMI. *Atmospheric Measurement Techniques*, *6*(10), 2607–2626. https://doi.org/10.5194/amt-6-2607-2013

Cho, Y., Kim, J., Go, S., Kim, M., Lee, S., Kim, M., Chong, H., Lee, W.-J., Lee, D.-W., Torres, O., & Park, S. S. (2024). First atmospheric aerosol-monitoring results from the Geostationary Environment Monitoring Spectrometer (GEMS) over Asia. *Atmospheric Measurement Techniques*, *17*(14), 4369–4390. https://doi.org/10.5194/amt-17-4369-2024

Committee on Earth Observation Satellites (CEOS). (2019). *Geostationary Satellite Constellation for Observing Global Air Quality: Geophysical Validation Needs Prepared by the CEOS Atmospheric Composition Virtual Constellation and the CEOS Working Group on Calibration and Validation*.

Douros, J., Eskes, H., van Geffen, J., Boersma, K. F., Compernolle, S., Pinardi, G., Blechschmidt, A.-M., Peuch, V.-H., Colette, A., & Veefkind, P. (2022). *Comparing Sentinel-5P TROPOMI NO2 column observations with the CAMS-regional air quality ensemble*. https://doi.org/10.5194/egusphere-2022-365

Edwards, D. P., Martínez-Alonso, S., Jo, D. S., Ortega, I., Emmons, L. K., Orlando, J. J., Worden, H. M., Kim, J., Lee, H., Park, J., & Hong, H. (2024). Quantifying the diurnal variation in atmospheric NO2 from Geostationary Environment Monitoring Spectrometer (GEMS) observations. *Atmospheric Chemistry and Physics*, *24*(15), 8943–8961. https://doi.org/10.5194/acp-24-8943-2024

Garane, K., Heue, K.-P., Verhoelst, T., Koukouli, M., Lambert, J.-C., & Balis, D. (2023). *PEGASOS Validation Report - Total Ozone*.

Inness, A., Aben, I., Ades, M., Borsdorff, T., Flemming, J., Jones, L., Landgraf, J., Langerock, B., Nedelec, P., Parrington, M., & Ribas, R. (2022). Assimilation of S5P/TROPOMI carbon monoxide data with the global CAMS near-real-time system. *Atmospheric Chemistry and Physics*, *22*(21). https://doi.org/10.5194/acp-22-14355-2022

Inness, A., Alben, I., Agusti-Panareda, A., Borsdoff, T., Flemming, J., Landgraf, J., & Ribas, R. (2019). Monitoring and assimilation of early TROPOMI total column carbon monoxide data in the CAMS system. In *ECMWF Technical Memoranda*.

Keppens, A., Di Pede, S., Hubert, D., Lambert, J. C., Veefkind, P., Sneep, M., De Haan, J., Ter Linden, M., Leblanc, T., Compernolle, S., Verhoelst, T., Granville, J., Nath, O., Fjæraa, A. M., Boyd, I., Niemeijer, S., Van Malderen, R., Smit, H. G. J., Duflot, V., … Zehner, C. (2024). 5 years of Sentinel-5P TROPOMI operational ozone profiling and geophysical validation using ozonesonde and lidar ground-based networks. *Atmospheric Measurement Techniques*, *17*(13), 3969–3993. https://doi.org/10.5194/amt-17-3969-2024

Kim, B.-R., Kim, G., Cho, M., Choi, Y.-S., & Kim, J. (2024). First results of cloud retrieval from the Geostationary Environmental Monitoring Spectrometer. *Atmospheric Measurement Techniques*, *17*(2), 453–470. https://doi.org/10.5194/amt-17-453-2024

Kim, J., Jeong, U., Ahn, M. H., Kim, J. H., Park, R. J., Lee, H., Song, C. H., Choi, Y. S., Lee, K. H., Yoo, J. M., Jeong, M. J., Park, S. K., Lee, K. M., Song, C. K., Kim, S. W., Kim, Y. J., Kim, S. W., Kim, M., Go, S., … Choi, Y. (2020). New era of air quality monitoring from space: Geostationary environment monitoring spectrometer (GEMS). *Bulletin of the American Meteorological Society*, *101*(1), E1–E22. https://doi.org/10.1175/BAMS-D-18-0013.1

Kim, S., Kim, D., Hong, H., Chang, L.-S., Lee, H., Kim, D.-R., Kim, D., Yu, J.-A., Lee, D., Jeong, U., Song, C.-K., Kim, S.-W., Park, S. S., Kim, J., Hanisco, T. F., Park, J., Choi, W., & Lee, K. (2023). First-time comparison between NO2 vertical columns from Geostationary Environmental Monitoring Spectrometer (GEMS) and Pandora measurements. *Atmospheric Measurement Techniques*, *16*(16), 3959–3972. https://doi.org/10.5194/amt-16-3959-2023

Lange, K., Richter, A., Bösch, T., Zilker, B., Latsch, M., Behrens, L. K., Okafor, C. M., Bösch, H., Burrows, J. P., Merlaud, A., Pinardi, G., Fayt, C., Friedrich, M. M., Dimitropoulou, E., Van Roozendael, M., Ziegler, S., Ripperger-Lukosiunaite, S., Kuhn, L., Lauster, B., … Lee, H. (2024). Validation of GEMS tropospheric NO2 columns and their diurnal variation with ground-based DOAS measurements. *Atmospheric Measurement Techniques*, *17*(21), 6315–6344. https://doi.org/10.5194/amt-17-6315-2024

Lange, K., Richter, A., Schönhardt, A., Meier, A. C., Bösch, T., Seyler, A., Krause, K., Behrens, L. K., Wittrock, F., Merlaud, A., Tack, F., Fayt, C., Friedrich, M. M., Dimitropoulou, E., Van Roozendael, M., Kumar, V., Donner, S., Dörner, S., Lauster, B., … Burrows, J. P. (2023). Validation of Sentinel-5P TROPOMI tropospheric NO2 products by comparison with NO2 measurements from airborne imaging DOAS, ground-based stationary DOAS, and mobile car DOAS measurements during the S5P-VAL-DE-Ruhr campaign. *Atmospheric Measurement Techniques*, *16*(5), 1357–1389. https://doi.org/10.5194/amt-16-1357-2023

Lee, H., Park, J., Hong, H., Kim, J., Lee, H.-J., Jung, Y., Roozendael, M. Van, Fayt, C., Park, R., Kim, S., Ahn, M.-H., Jacob, D. J., Kim, D., Choi, W., Lee, W.-J., Lee, D.-W., Wagner, T., Richter, A., Krotkov, N. A., & Lamsal, L. N. (2024, March 12). *Diurnal characteristics of the NO2 columns observed over Asia from Geostationary Environment Monitoring Spectrometer (GEMS)*. https://doi.org/10.5194/egusphere-egu24-17722

Lee Hanlim, Park Junsung, & Hong Hyunkee. (2020). *Geostationary Environment Monitoring Spectrometer (GEMS) Algorithm Theoretical Basis Document NO2 Retrieval Algorithm*.

Lee, K., Lee, D. W., Chang, L. S., Yu, J. A., Lee, W. J., Kang, K. H., & Jeong, J. (2024). Pioneering Air Quality Monitoring over East and Southeast Asia with the Geostationary Environment Monitoring Spectrometer (GEMS). In *Korean Journal of Remote Sensing* (Vol. 40, Issue 5, pp. 741–752). Korean Society of Remote Sensing. https://doi.org/10.7780/kjrs.2024.40.5.2.5

Levelt, P. F., van den Oord, G. H. J., Dobber, M. R., Malkki, A., Huib Visser, Johan de Vries, Stammes, P., Lundell, J. O. V., & Saari, H. (2006). The ozone monitoring instrument. *IEEE Transactions on Geoscience and Remote Sensing*, *44*(5), 1093–1101. https://doi.org/10.1109/TGRS.2006.872333

Li, Y., Xing, C., Peng, H., Song, Y., Zhang, C., Xue, J., Niu, X., & Liu, C. (2023). Long-term observations of NO2 using GEMS in China: Validations and regional transport. *Science of the Total Environment*, *904*. https://doi.org/10.1016/j.scitotenv.2023.166762

Lorente, A., Folkert Boersma, K., Yu, H., Dörner, S., Hilboll, A., Richter, A., Liu, M., Lamsal, L. N., Barkley, M., De Smedt, I., Van Roozendael, M., Wang, Y., Wagner, T., Beirle, S., Lin, J. T., Krotkov, N., Stammes, P., Wang, P., Eskes, H. J., & Krol, M. (2017). Structural uncertainty in air mass factor calculation for NO2 and HCHO satellite retrievals. *Atmospheric Measurement Techniques*, *10*(3). https://doi.org/10.5194/amt-10-759-2017

Lutz, R., Loyola, D. G., Zehner, C., Lee, W.-J., & Kim, J. (2023). Overview of the PEGASOS Project for Evaluation of the Operational GEMS L2 Products. *AGU Fall Meeting Abstracts*, *2023*, A33D-07.

Park, S. S., Kim, J., Cho, Y., Lee, H., Park, J., Lee, D.-W., Lee, W.-J., & Kim, D.-R. (2023, July 4). *Retrieval Algorithm for Aerosol Effective Height from the Geostationary Environment Monitoring Spectrometer (GEMS)*. https://doi.org/10.5194/amt-2023-136

Richter, A., Lange, K., Burrows, J. P., Boesch, H., Kim, S.-W., Seo, S., Kim, K.-M., Hong, H., Lee, H., & Park, J. (2024, November 27). *The GEMS IUP-UB tropospheric NO2 product - sensitivity studies and first results*. https://doi.org/10.5194/egusphere-egu24-10221

Seo, S., Kim, S.-W., Kim, K.-M., Richter, A., Lange, K., Burrows, J. P., Park, J., Hong, H., Lee, H., Jeong, U., & Kim, J. (2024). *Diurnal variations of NO2 tropospheric vertical column density over the Seoul Metropolitan Area from the Geostationary Environment Monitoring Spectrometer (GEMS): seasonal differences and impacts of varying a priori NO2 profile data*. https://doi.org/10.5194/amt-2024-33

Seo, S., Valks, P., Lutz, R., Heue, K.-P., Hedelt, P., Molina García, V., Loyola, D., Lee, H., & Kim, J. (2024). Tropospheric NO2 retrieval algorithm for geostationary satellite instruments: applications to GEMS. *Atmospheric Measurement Techniques*, *17*(20), 6163–6191. https://doi.org/10.5194/amt-17-6163-2024

van Geffen, J., Eskes, H., Compernolle, S., Pinardi, G., Verhoelst, T., Lambert, J.-C., Sneep, M., ter Linden, M., Ludewig, A., Boersma, K. F., & Veefkind, J. P. (2022). Sentinel-5P TROPOMI NO2 retrieval: impact of version v2.2 improvements and comparisons with OMI and ground-based data. *Atmospheric Measurement Techniques*, *15*(7), 2037–2060. https://doi.org/10.5194/amt-15-2037-2022

Veefkind, J. P., Aben, I., McMullan, K., Förster, H., de Vries, J., Otter, G., Claas, J., Eskes, H. J., de Haan, J. F., Kleipool, Q., van Weele, M., Hasekamp, O., Hoogeveen, R., Landgraf, J., Snel, R., Tol, P., Ingmann, P., Voors, R., Kruizinga, B., … Levelt, P. F. (2012). TROPOMI on the ESA Sentinel-5 Precursor: A GMES mission for global observations of the atmospheric composition for climate, air quality and ozone layer applications. *Remote Sensing of Environment*, *120*, 70–83. https://doi.org/10.1016/j.rse.2011.09.027

Veefkind, P., Leune, B., Van Geffen, J., & Hong, H. (2024). *Comparing TROPOMI and GEMS Observations for the Same Sun-Satellite geometry*. https://doi.org/https://doi.org/10.5194/egusphere-egu24-10909

Zhang, Y., Lin, J., Kim, J., Lee, H., Park, J., Hong, H., Van Roozendael, M., Hendrick, F., Wang, T., Wang, P., He, Q., Qin, K., Choi, Y., Kanaya, Y., Xu, J., Xie, P., Tian, X., Zhang, S., Wang, S., … Liu, M. (2023). A research product for tropospheric NO2 columns from Geostationary Environment Monitoring Spectrometer based on Peking University OMI NO2 algorithm. *Atmospheric Measurement Techniques*, *16*(19), 4643–4665. https://doi.org/10.5194/amt-16-4643-2023

Document History

Version	Author(s)	Date	Changes
1.0	Paschalidi, Inness, Huijnen	25.11.2024	Initial version
2.0	Paschalidi, Inness, Huijnen	16.12.2023	Revised version

Internal Review History

Internal Reviewers	Date	Comments
Segers, A.J.	09.12.2024	
Remy, S.	09.12.2024	